Engineering Structures 335 (2025) 120392

Contents lists available at ScienceDirect

Engineering Structures

journal homepage: www.elsevier.com/locate/engstruct

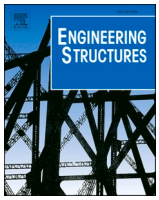

Performance of single and built-up I-shaped cold formed steel stud under double sided walls fire exposure

Mohammed Hassoune [a], Abdelhak Kada [a], Belkacem Menadi [b], Belkacem Lamri [a], Ouissam Yessad [a], Paulo A.G. Piloto [c,*], Liming Jiang [d]

[a] Laboratory Fire Safety Engineering of Constructions and Protection of their Environment (LISICPE), Faculty of Civil Engineering and Architecture, Hassiba Benbouali University of Chlef, Chlef, Algeria
[b] Laboratory of Geo-Materials and Civil Engineering, Department of Civil Engineering, University of Blida 1, Blida, Algeria
[c] GICoS, Instituto Politécnico de Bragança, Bragança, Portugal
[d] Department of Building Environment and Energy Engineering, The Hong Kong Polytechnic University, Hung Hom, Kowloon, Hong Kong

ARTICLE INFO

Keywords:
Light gauge steel frame (LSF) walls
Cold formed steel (CFS)
Web stiffeners
Built-up I-shaped
Numerical modelling
Fire resistance

ABSTRACT

Light-gauge Steel Frame (LSF) walls are expanded nowadays due to several advantages, especially to achieve economy, sustainability and improved structural performance. The latter has stimulated designers to adopt Cold Formed Steel (CFS) members as primary components of LSF walls. However, the high thermal conductivity and slenderness of CFS sections make them vulnerable to mechanical degradation during fire. While numerous studies have investigated the performance of CFS stud walls under one-sided fire exposure, the investigation on double-sided fire exposure remains limited, especially for built-up studs. This study investigates the performance of CFS stud walls under compression loading, subjected to one-sided and double-sided fire exposure. Numerical models were developed using ANSYS APDL, considering geometric imperfections, material nonlinearities and contact element effect. The developed models were validated against previous experimental and numerical results. Various parameters were analysed through parametric study, including steel thickness and grades, web stiffeners and I-shaped stud configurations. The results demonstrate the significant impact of the double-sided fire exposure on CFS walls performance, reducing the fire resistance by 41 % and 50 % for CFS thicknesses of 1.15 mm and 1.5 mm, respectively, compared to one-sided fire exposure. Steel grade and I-shaped configurations were found to significantly enhance the load-bearing capacity and fire resistance of CFS walls. The maximum temperatures predicted for each load ratio were used to calculate the load ratio as per EN1993–1–2. New formulas, based on load ratio were proposed to predict the maximum temperature at failure for CFS walls subjected to one-sided and double-sided fire exposure. The findings will improve fire structural design codes of CFS walls, by ensuring accurate predictions of limiting temperatures and fire resistance and providing engineers with substantial data for LSF structures.

1. Introduction

Light-gauge Steel Framing (LSF) walls made of Cold-Formed Steel (CFS) members have been increasingly adopted as a sustainable alternative to traditional masonry or concrete walls, motivated by the need to decrease the weight of the structure [1]. Given the versatility of using CFS section, the most important advantage for structural design is the strength to weight ratio, which is typical for CFS thin-walled members [2,3]. Due to their low thickness-to-width ratio, the web buckling, distortional buckling and the other different buckling modes may occur, as specified by Vlasov thin-walled member's theory [4]. Further, the vulnerability of steel and LSF walls to fire is a critical concern as steel is susceptible to the degradation of mechanical properties at elevated temperatures due to its high thermal conductivity [5,6]. CFS, in particular, is more significantly affected by high temperatures because of their slenderness and high shape factor. Over the last years, several research works, including experimental tests [7–12] and numerical simulations [13–18], have focused on enhancing the fire resistance of CFS walls by including various types of external fire protection and cavity insulation used in different wall configurations. Most results have

* Corresponding author.
E-mail address: ppiloto@ipb.pt (P.A.G. Piloto).

https://doi.org/10.1016/j.engstruct.2025.120392
Received 28 January 2025; Received in revised form 24 March 2025; Accepted 16 April 2025
Available online 18 April 2025

shown that the fire resistance can be improved by doubling the protective layers and the positioning of external insulation, sandwiched between two protective layers, rather than placing it in the cavity region. Also, previous researches on the fire performance of CFS center-sheathed shear walls [19] have shown that the vertical load ratio significantly influences fire resistance, more so than the lateral load ratio. Furthermore, the inclusion of an interior stud has been found to improve the fire resistance of the wall, while the aspect ratio appears to have a negligible effect. However, some studies [20,21] have indicated that the recommended critical temperature (350°C) of EN1993–1–2 [22] could be unsafe in case of load-bearing LSF walls, highlighting the need for more investigations on this research topic. Various types of built-up CFS stud configurations have also been investigated both at ambient temperature [23–26] and only recently under fire conditions [27–29] to address the need for enhanced fire resistance and increased load-bearing capacity of CFS studs walls. Some findings indicated that Back-to-Back (B-B) and Nested Channel (NC) studs exhibited similar fire behaviour to those of single studs in case of absence of cavity insulation inside of the panel. However, NC stud walls were notably affected by the inclusion of cavity insulation, leading to an enhanced fire resistance level. Other results showed that the NC stud can provide higher fire performance compared to Face-to-Face (F-F) studs. Recent studies have investigated the flexural behaviour of galvanised CFS B-B built-up beams at elevated temperatures, considering the impact of different cooling methods [30] and the different stiffener configurations [31]. The results indicate that the water-cooling method exhibited slightly lower load-bearing capacity compared to the air-cooling method when heated to the same temperature. Furthermore, beams with vertical stiffeners demonstrated improved structural performance compared to those with horizontal stiffeners. Few research studies have investigated the influence of incorporating web-stiffeners to evaluate the fire performance of CFS stud walls under axial compression load [32–34]. These studies demonstrated that while including web-stiffeners significantly increases the load-bearing capacity of CFS studs, it can also reduce the fire resistance. However, due to the limited research on web-stiffened CFS studs under fire conditions, significant gaps remain in understanding their fire performance comprehensively. The behaviour of CFS walls with web-stiffened studs is not yet fully understood, especially given the diverse types and shapes of stiffeners that can be adopted, either for single studs or even for built-up sections. Recent literature has predominantly focused on the fire performance of LSF systems under one-sided fire exposure, as detailed above, and only few research studies have addressed the behaviour of LSF walls under both-sided fire exposure [35–37]. Thus, significant research is needed for stud element frame to bridge the gap in understanding the double-sided fire response of CFS wall systems, particularly when being used as internal walls within compartments completely engulfed in flames. More experimental and numerical data are required to address this fire exposure scenario, which presents a special concern to the industry [38], especially for web-stiffened and I-shaped built-up stud configurations.

The present research work extends past research by addressing the gaps in the behaviour of CFS walls under compression loading, particularly when exposed to fire on both sides. While web stiffeners and doubling the stud into an I-shaped configuration have been shown to enhance the load-bearing capacity of CFS walls at ambient temperature, their behaviour under elevated temperatures remains insufficiently explored. It also provides a new insight especially for the case of CFS walls with double-sided fire exposure comprising built-up studs and stiffened sections.

It also aims to fill a major gap to understand the failure mechanisms and load-bearing capacity of CFS walls, considering the influence of built-up stud configurations, stiffeners and the number of faces simultaneously exposed to fire.

The developed FE models for single and built-up sections were validated and calibrated at room temperature and under fire scenarios, using experimental and numerical data available in the literature, considering geometric imperfections, material nonlinearities and contact element effect. A parametric analysis was developed to study the influence of steel grade and thickness, web stiffeners on the behaviour of CFS stud walls under an axial compression load, subjected to fire on both one side and two sides of the wall. Significant insights have been gained regarding the fire resistance and the maximum temperature of the various CFS wall types, with a load ratio ranging from 0.2 to 0.8. The findings also highlighted the pronounced impact of double-sided fire exposure on the thermal and structural performance of CFS walls compared to one-sided fire exposure. The results contribute to improving safer construction design by evaluating the maximum temperature under both one-sided and double-sided fire exposure, and proposing new formulas for predicting failure temperatures based on load ratio correlation.

2. Study cases for CFS stud walls

The LSF wall assembly examined in this study, as detailed by Piloto et al. [21], is a reduced-scale specimen measuring 1000 mm in height and 975 mm in width, built using two types of CFS members, both of S280GD+Z steel grade. The primary structural components consist of five C90x43x15 × 1.5 mm Lipped Channel Studs (LCS), spaced at regular intervals of 233 mm, and connected with U93x43x1.5 mm tracks. This frame specimen is protected on both sides by a single layer of 12.5 mm thick plasterboard, with screws spaced at 152 mm apart, securing the boards to the studs. It is worth mentioning that the number of components and interactions between multiple elements and materials, such as studs-to-tracks or studs-to-boards, present significant challenges to numerical analyses, particularly in the context of structural analyses. These features contribute to the overall high complexity of the numerical investigation of the entire wall panel. To mitigate these challenges and accurately simulate the fire behaviour of the LSF walls, the middle stud, identified as the most critical element, was isolated from the wall panel. This approach allows for a more detailed analysis of the critical factors affecting the stud's performance under fire. The details and dimensions of the investigated LSF wall and the isolated CFS stud are illustrated in Fig. 1.

Several other models are examined to investigate the effects of different structural parameters on the performance of CFS stud walls at room temperature, under one-sided and double-sided fire exposure. This study considers six LCS models to assess the influence of stud thickness and grade on the thermal and structural behaviour of CFS stud walls, including three different thicknesses and three different steel grades, see Table 1. The LCS model is further modified to include stiffeners, such as Single Web Stiffener (SWS), Double Web Stiffeners (DWS) and Omega-Web Stiffeners (OWS), as shown in Fig. 2. These models are doubled as B-B stud, as detailed in Fig. 3 and Table 1, with stud-to-stud screws spaced identically to stud-to-board screws. The objective of using these I-shaped configurations is to evaluate the impact of the enhanced strength and stability on the fire performance of CFS stud walls.

3. Thermal and mechanical properties of CFS walls at elevated temperatures

The thermal conductivity (λ_a) and specific heat (c_a) of CFS steel, presented in Fig. 4(a), were defined according to EN1993–1–2 [22]. The CFS density (ρ_a) at room temperature is assumed to be 7850 kg/m^3 and remains constant at elevated temperatures. The plasterboard is used as an external protection to delay the rise in temperature within the CFS surfaces. The thermal conductivity (λ_p), specific heat (c_p) and density (ρ_p) of plasterboard were obtained as reported in the study of Dodangoda et al. [39], as shown in Fig. 4(b).

Both thermal properties account for physical events and are assumed to be the effective thermal properties. The transition temperature in steel is used to simulate the phase transition from ferrite to austenite, assuming an endothermic event represented by the variation of the

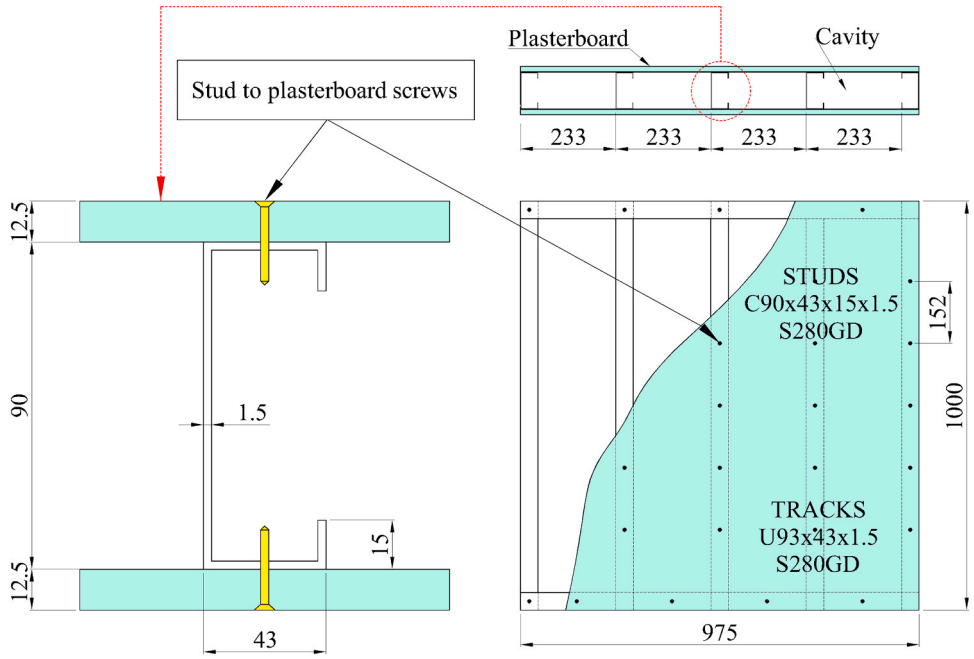

Fig. 1. Details and dimensions of investigated LSF wall panel [21].

specific heat. The transition temperature in the gypsum plasterboard around 100–200 °C is related to the vaporisation of the free water and is represented by the variation of the specific heat. The conductivity is also increasing after 900 °C to account for the thermal degradation of the material.

The yield stress at room temperature was selected based on the nominal material strength of the different steel grades used in this study, in accordance with EN1993–1–3 [40], with a consistent elastic modulus of 210 GPa. The mechanical properties at elevated temperatures, including the yield stress and the elastic modulus, were calculated using the reduction factors proposed by Kankanamge and Mahendran [41]. The Poisson's ratio was assumed as 0.3 and remained constant at elevated temperatures. The thermal expansion coefficient provided by EN1993–1–2 [22], was included in the numerical models. The reduced mechanical properties were used to determine the stress-strain curve at each temperature level for a given stress, as shown in Fig. 5. These curves are based on strain hardening material models, known as the Ramberg-Osgood model, which assumes the existence of the strain hardening in the inelastic phase instead of constant yield stress in all plastic phase. The engineering stress-strain values were converted to true-stress (σ_{true}) and logarithmic plastic strain ($\varepsilon^{pl}{}_{true}$) using Eq. (1).

$$\sigma_{true} = \sigma_{eng}(1+\varepsilon_{eng}) \text{and} \varepsilon^{pl}{}_{true} = \ln(1+\varepsilon_{eng}) - \frac{\sigma_{true}}{E} \quad (1)$$

4. Numerical modelling and analysis strategy

This research study is based on Finite Element Method (FEM) using ANSYS APDL software [42], conducted for four step solution methods. (i) Eigen buckling analysis was performed first to determine the critical buckling load of the CFS stud and to extract the associated instability mode. (ii) Nonlinear static structural analysis was conducted in the second step to predict the load-bearing capacity of CFS stud wall at room temperature, taking into account the geometric imperfections effect. (iii) The third step used a nonlinear transient heat transfer analysis under fire ISO834 to evaluate the thermal effect and conclude the time-temperature profiles. (iv) Sequentially coupled thermal-structural analysis was developed at the final step, using material and geometry nonlinearities effect at high temperatures, and the temperature distribution obtained from the thermal analysis to predict the fire resistance and the maximum temperature.

4.1. Finite element type selection

SHELL131 which features four nodes and SHELL132 which includes eight nodes were used for single and built-up stud thermal models, respectively, with each node having 32 temperature degrees of freedom maximum (layered finite element). SHELL132 is specifically designed to handle contact and gap elements, where interactions between surfaces need to be considered. The plasterboard was modelled with SOLID70, which has eight nodes, and was used in conjunction with SHELL131, while SOLID90, featuring twenty nodes, was paired with SHELL132. These two elements assigned with a single degree of freedom, temperature, at each node. Then, SHELL131 and SHELL132 are switched to SHELL181 and SHELL281, respectively, for modelling CFS mechanical models. These mechanical SHELL elements have six degrees of freedom at each node, including translations in X, Y, and Z directions, and rotations about X, Y, and Z axes. BEAM188 elements are employed to represent the stud-to-stud screws. It is particularly effective for modelling the connection stiffness and load transfer characteristics between studs. Plasterboard layers were excluded to simplify the mechanical analysis, focusing solely on evaluating the structural performance of the CFS steel and the overall stud configuration, but including the lateral restrain produced by the connecting screws used to fix the plasterboard layers. It is worth mentioning that the effects of curvature of the corner regions and their strength enhancements are generally minimal due to the slenderness of the CFS section and the small corner radius. Therefore, they were not explicitly considered in the numerical modelling to simplify the FE model and mitigate computational complexity, as adopted in several past numerical studies [29,33,43].

4.2. Contact interaction

The accurate modelling of contact interactions is crucial for reliable simulation results. Several issues, such as the interpenetration of shell elements, may arise from selecting an inappropriate contact type between the target surface and the contact surface, leading to non-physical behaviour and instabilities producing inaccurate solutions. Additionally, neglecting friction between the web surfaces can modify the

Table 1
Configuration details of investigated single LCS and built-up I-shaped stud.

Stud configurations	Models	Thickness [mm]	Steel grade [MPa]
Single unstiffened	LCS−1.15	1.15	280
Single unstiffened	LCS−1.5	1.5	280
Single unstiffened	LCS−2.5	2.5	280
Single unstiffened	LCS-S220	1.5	220
Single unstiffened	LCS-S280	1.5	280
Single unstiffened	LCS-S350	1.5	350
Single web-stiffened	LCS-SWS−1.15	1.15	280
Single web-stiffened	LCS-DWS−1.15	1.15	280
Single web-stiffened	LCS-OSS−1.15	1.15	280
Single web-stiffened	LCS-SWS−1.5	1.5	280
Single web-stiffened	LCS-DWS−1.5	1.5	280
Single web-stiffened	LCS-OSS−1.5	1.5	280
Single web-stiffened	LCS-SWS−2.5	2.5	280
Single web-stiffened	LCS-DWS−2.5	2.5	280
Single web-stiffened	LCS-OSS−2.5	2.5	280
Unstiffened Built-up I-shaped	B-B-LCS−1.15	1.15	280
Web-stiffened Built-up I-shaped	B-B-SWS−1.15	1.15	280
Web-stiffened Built-up I-shaped	B-B-DWS−1.15	1.15	280
Web-stiffened Built-up I-shaped	B-B-OWS−1.15	1.15	280
Unstiffened Built-up I-shaped	B-B-LCS−1.5	1.5	280
Web-stiffened Built-up I-shaped	B-B-SWS−1.5	1.5	280
Web-stiffened Built-up I-shaped	B-B-DWS−1.5	1.5	280
Web-stiffened Built-up I-shaped	B-B-OWS−1.5	1.5	280
Unstiffened Built-up I-shaped	B-B-LCS−2.5	2.5	280
Web-stiffened Built-up I-shaped	B-B-SWS−2.5	2.5	280
Web-stiffened Built-up I-shaped	B-B-DWS−2.5	2.5	280
Web-stiffened Built-up I-shaped	B-B-OWS−2.5	2.5	280

interaction of the stud members. While nonzero coefficients of friction can improve the real behaviour of the CFS stud wall, they also introduce numerical complexity that may lead to some convergence difficulties in FEM. Therefore, in order to represent the interaction relationship between the webs in I-shaped configuration, and to prevent the interpenetration of the two studs' shell elements, a surface-to-surface interaction based on standard contact behaviour was applied. This contact was modelled using CONTA and TARGE elements, which are specifically developed for managing contact and target surfaces in ANSYS. The CONTA174 elements were assigned to one surface of the web stud, while TARGE170 elements were assigned to the corresponding contact surface of the adjacent web stud. The friction coefficient between the contact surfaces was set to 0.19, which is a common value used for steel-to-steel interactions [23]. Furthermore, neither stud-to-board nor stud-to-stud screws were included in the thermal analysis, considering perfect contact between plasterboard SOLID and stud SHELL elements.

4.3. Boundary conditions, load application and mesh sensitivity

Convection and radiation were applied as primary thermal boundary conditions according to EN-1991–1–2 [44], with a heat transfer coefficient of 25 W/m^2K on the fire-exposed side of plasterboard, and 9 W/m^2K on the unexposed side, which accounts for the radiation effect. Additionally, the heat transfer due to thermal radiation on both the fire-exposed side and within the panel cavity was incorporated into the CFS thermal model. A flame emissivity factor of 1.0 was applied with a Stefan-Boltzmann constant of 5.67×10^{-8} W/m^2K^4 [42], as used in numerous previous studies [15,20,21]. The bulk temperature is applied on the exposed side as time-temperature relationship according to ISO834 fire, assuming a constant room temperature of 20°C on the unexposed side. Fig. 6 shows the details of applied thermal boundary conditions on the CFS stud wall model under both fire scenarios. The thermal analysis was conducted as a nonlinear transient analysis, selecting the full option settings with a time step size of 60 s and a minimum and maximum time step of 1 s and 60 s, respectively. The solution convergence was based on the heat flow criterion, considering a tolerance value of 10^{-3} and a reference value of 10^{-6} W.

The structural analysis of the CFS stud walls was conducted under pinned end conditions restraining the ends of the studs in the (UX), (UY) displacements, and the (RZ) rotation at the centroid of the cross-section, where the axial load was applied as shown in Fig. 7. At the opposite end of the stud, similar restraints were applied, with the additional constrained of (UZ) displacement. To ensure accurate load transfer and distribution, these boundary conditions were applied to a master node at each end of the stud. This master node was then coupled to all nodes along the end section of the stud, defining a rigid region (CE). The effect of the stud-to-board screw connections was incorporated by introducing in-plane lateral restraints (UX) at the screw positions. An additional constraint of the (UY) displacement was applied for the built-up stud validation model (full scale model) to account for the effect of out-of-plane lateral restraints, which could also be provided by the stud-to-board screws, as recommended by Vieira Jr and Schafer [45]. However, since the reduced scale CFS stud models were not susceptible to the

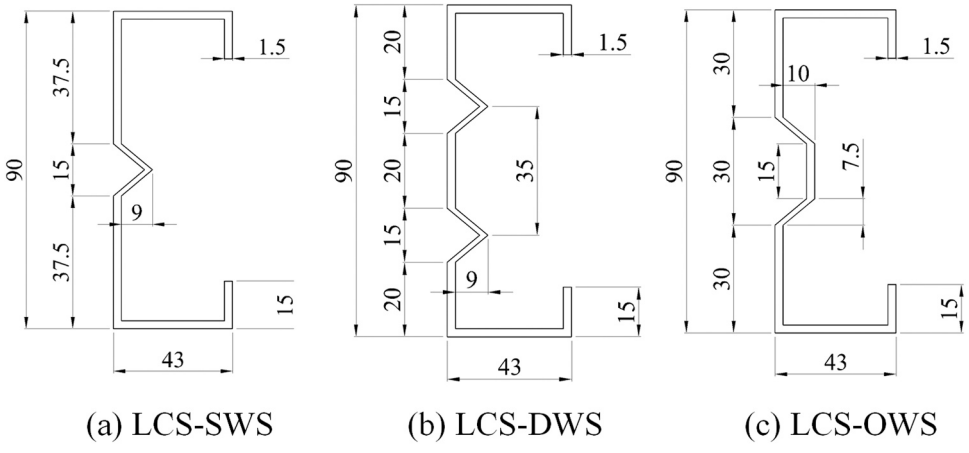

Fig. 2. Configurations of stiffeners within the LCS web.

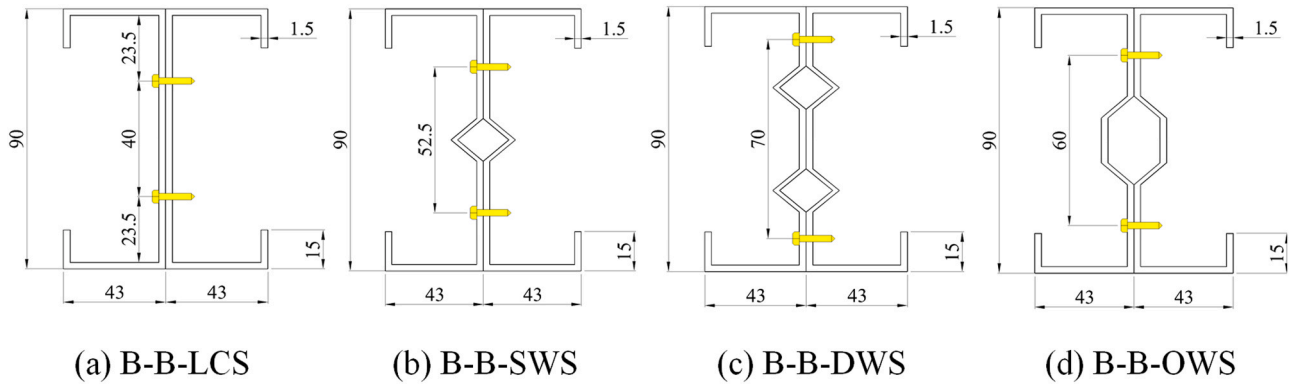

Fig. 3. Built-up I-shaped stud configurations.

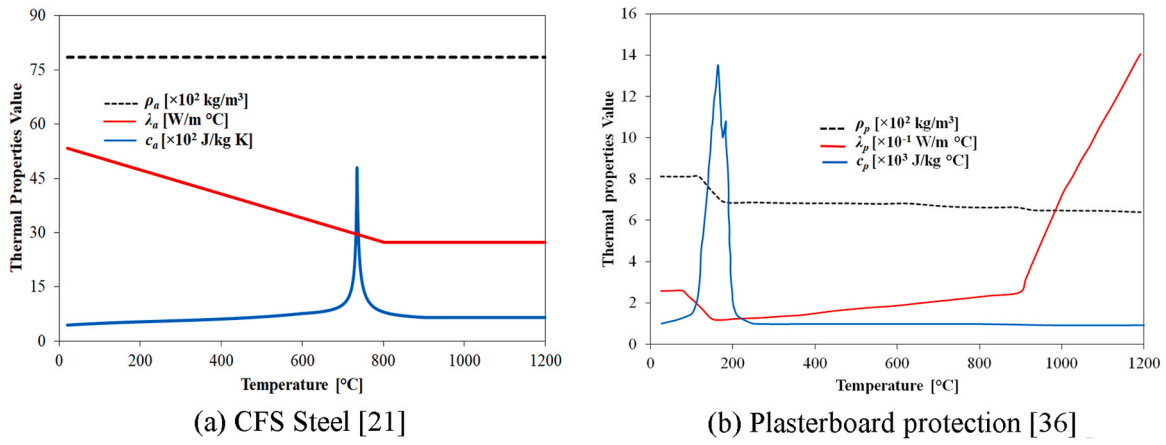

Fig. 4. Variation of thermal material properties at elevated temperatures.

out-of-plane deviation, this lateral restraint was excluded to simplify the FE models. A mesh sensitivity analysis was conducted by testing various mesh sizes, including 15 mm, 10 mm, 8 mm, 6 mm, 5 mm, and 4 mm as presented in Fig. 8. The convergence criterion was based on the comparison of the predicted ultimate failure load with those obtained from previous experimental study of Kolarkar [7] and Vy and Mahendran [25], for both single and built-up I-shaped stud configurations, respectively. The mesh was considered to have converged the solution when further refinement did not significantly change the predicted failure load. It was observed that while reducing the mesh size from 15 mm to 5 mm improved accuracy, refining it further to 4 mm produced identical results. Therefore, a 5 mm mesh size was selected as the optimal refinement for all numerical models, including the plasterboard layers.

4.4. Geometric imperfections and residual stresses

In this study, a linear elastic buckling analysis was performed using both the Block Lanczos solution method [42], which employs an automated shift strategy to extract the desired eigen-values using ANSYS [42], and the signature curve generated by CUFSM [46]. These methods are used to determine the critical buckling loads (F_{cr}) and their associated buckling modes, (Table 2). The CFS stud FE models used for the numerical eigen-buckling analysis were based on the same boundary conditions applied to the nonlinear models, excluding all lateral restraints along the stud length.

The consideration of geometric imperfections in the numerical models was based on prior research and the observed buckling modes from CUFSM [46]. For full-scale single stud models, Vy et al. [36] indicated that global imperfections have a negligible effect under one-sided fire exposure due to the dominance of thermal bowing caused by non-uniform temperature distribution. However, under both-sided fire exposure, global imperfections become more significant. To ensure consistency in numerical results, particularly at ambient temperature, both global and local imperfections were included into the models as recommended by Becque [47] without conducting an imperfection sensitivity analysis. For the full-scale built-up I-shaped stud, Vy and Mahendran [25] emphasised the necessity of incorporating both global (in-plane and out-of-plane) and local imperfections. Additionally, an imperfection sensitivity analysis was performed to assess the effect of including distortional buckling. The results showed that incorporating distortional imperfections led to a 4.6 % difference in the ultimate failure load compared to models without them. Furthermore, including distortional imperfections improved the agreement between experimental and numerical results, reducing the difference in ultimate failure load to less than 1 %. Consequently, distortional imperfections were also included in the full-scale I-shaped models. For the reduced-scale models, CUFSM was used to identify the dominant buckling modes. The results indicated that unstiffened LCS models (single and I-shaped) were governed solely by local buckling, (Fig. 9(a)), as observed in the study of Piloto et al. [21], while stiffened LCS models exhibited predominant distortional buckling, (Fig. 9(b)). Therefore, conducting an imperfection sensitivity analysis was deemed unnecessary for the reduced-scale models. The maximum local imperfection amplitude were introduced with an amplitude of 0.006 H, as recommended by Schafer and Peköz [48], where H is the web depth of the stud, and a global imperfection amplitude of L/1000, as noted in AS/NZS4600 [49]. The distortional geometric imperfections were incorporated with a maximum amplitude equivalent to the section thickness [48].

Lastly, residual stresses are negligibly small in magnitude for CFS

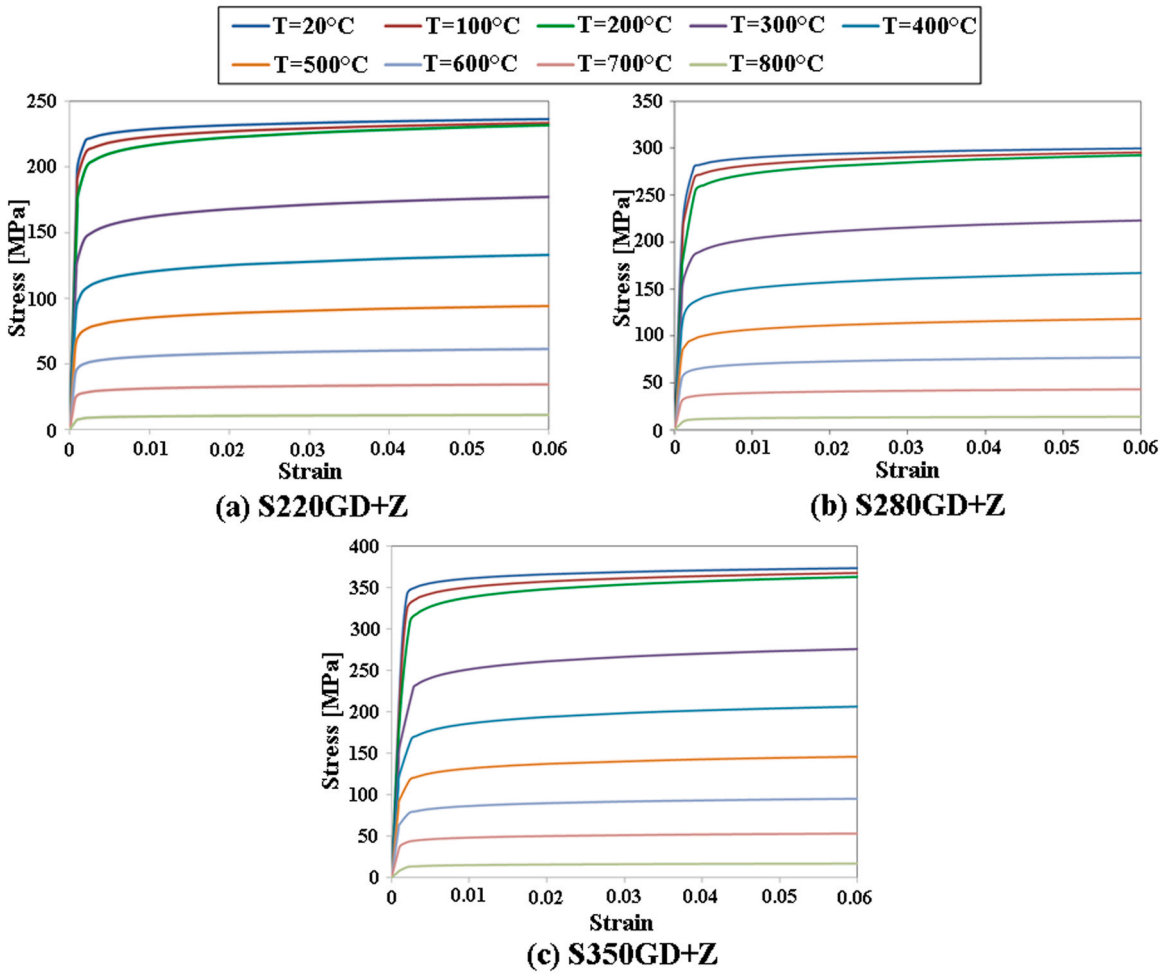

Fig. 5. Stress-Strain relationship for CFS steel.

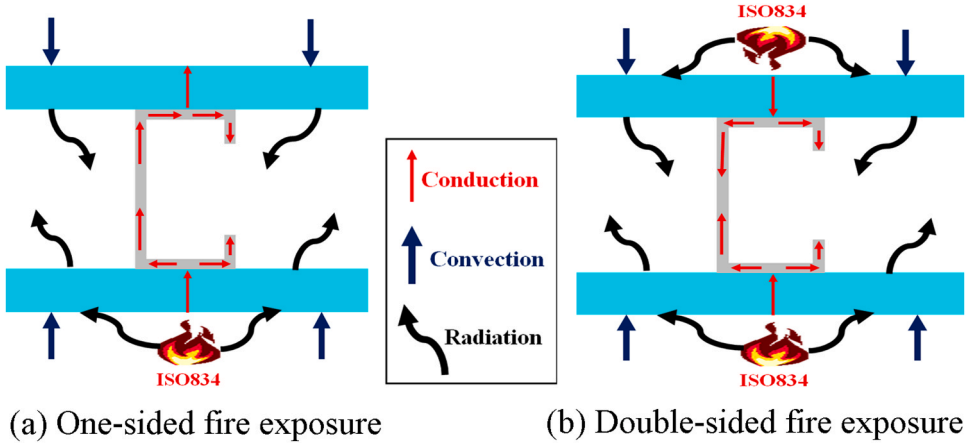

Fig. 6. Thermal boundary conditions.

since their manufacturing process does not involve any heat treatment or welding phase. According to several studies [48,50], compression-induced membrane residual stresses reduce compressive strength, particularly in corner regions where the yield stress is expected to be higher due to the cold work of forming. These opposing effects are often considered to counterbalance each other and should, therefore either be included or excluded together in the FE models. Additionally, Gunalan [51] investigated the effect of residual stresses on the ultimate load of CFS stud walls at ambient temperature. The results showed a minimal difference (approximately 0.5 %) between the ultimate loads obtained with and without residual stresses, suggesting an even lower impact at elevated temperature. Thus including residual stresses in CFS-FE models may unnecessarily complicate the analysis without significantly improving the accuracy of the results. Therefore, the effects of residual stresses were ignored as many previous numerical studies [29,36,43].

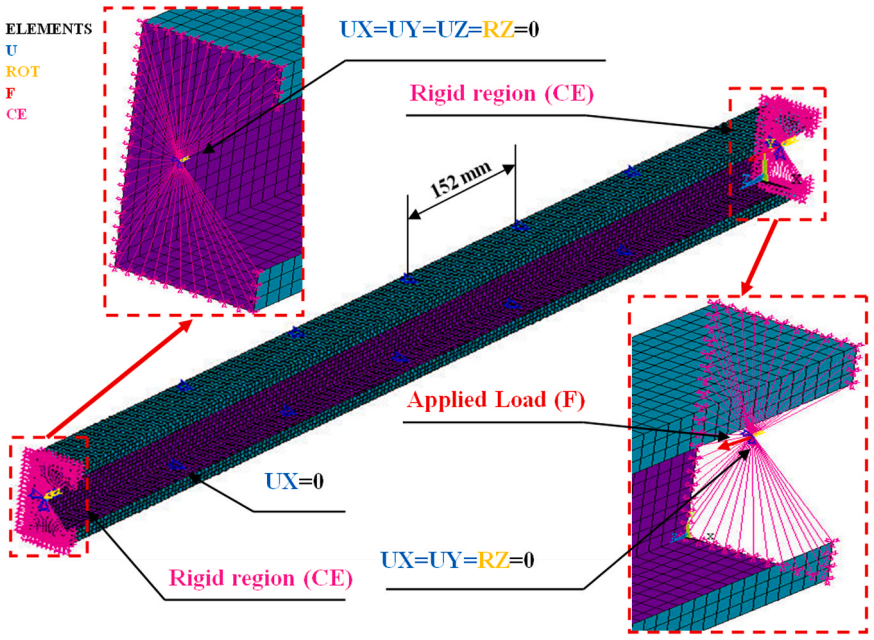

Fig. 7. Mesh size and structural boundary conditions used for the nonlinear stud models.

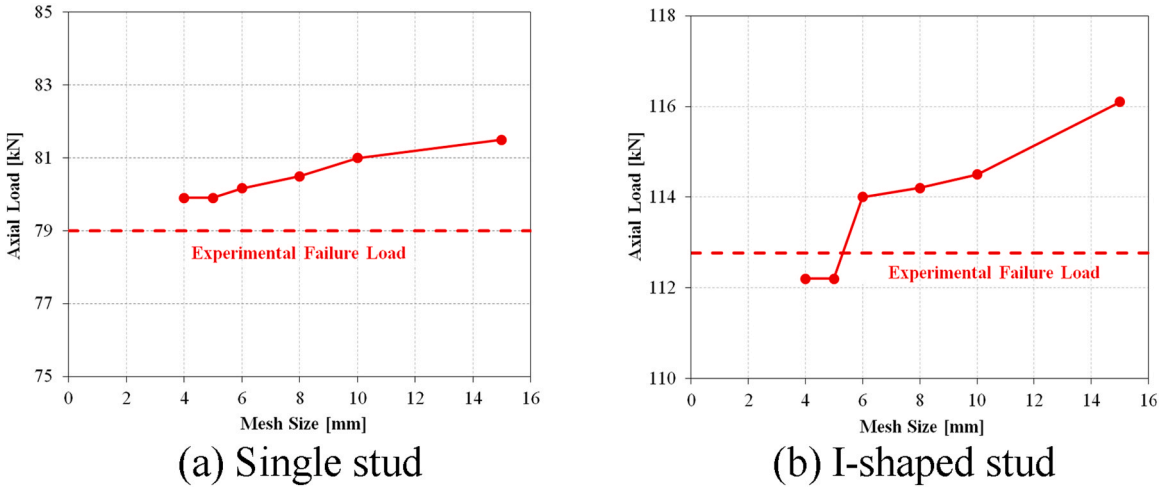

Fig. 8. Effect of mesh size on load-bearing capacity of CFS studs.

5. A thorough validation at ambient and under fire condition

5.1. Validation of structural FE model at room temperature

The validation process was conducted employing the Arc-Length method [42] to predict the load-bearing capacity, with an initial incremental load of 2 kN. This increment could vary during the solution process based on the maximum and minimum multipliers set to 25 and 0.0001, respectively. The convergence criterion was based on displacement with a tolerance value of 5 % and a reference value of 10^{-3} m. The single LCS and I-shaped stud were validated using the experimental results from Kolarkar [7] who reported an ultimate failure load of 79 kN, and Vy and Mahendran [25] who recorded a failure load of 112.77 kN, respectively. The CFS wall and the stud cross-section are detailed in their studies [7,25]. The developed numerical models predicted an ultimate load of 79.8 kN and 112.2 kN, for single and I-shaped stud, respectively, resulting in a negligible difference of only 1 %, confirming the accuracy of the FEA model to predict the failure ultimate load. Additionally, the load versus axial-shortening curves obtained from the ANSYS simulation were compared to those reported in the numerical studies by Gunalan [51] and Rokilan and Mahendran [43] for singe LCS (Fig. 10 (a)), and Vy and Mahendran [25] for I-shaped stud, (Fig. 10 (b)). The Root Mean Square Error (RMSE), calculated according to Eq. (2), was used as a statistical measure to validate the accuracy of the numerical models. The RMSE provides a quantitative assessment of the average difference between the predicted results (ANSYS) and the existing results (test/FEA from literature) for each corresponding chosen variant (n).

$$RMSE = \sqrt{\frac{1}{n}\sum_{i=1}^{n}[R_{FEA} - R_{test}]^2} \quad (2)$$

The RMSE is calculated for each 5 kN increment until failure for both stud configurations. However, due to the incomplete post-failure data from ANSYS for I-shaped stud, the RMSE is computed only up to the last predicted load. The RMSE values for axial shortening of the developed structural models are presented in Table 3. A good agreement was observed between all curves, with the maximum RMSE value not

Table 2
Comparison of the critical loads obtained from CUFSM and those from ANSYS.

Models	Buckling mode	$F_{cr\ (ANSYS)}$ [kN]	$F_{cr\ (CUFSM)}$ [kN]	$F_{cr\ (CUFSM)}$ / $F_{cr\ (ANSYS)}$
LCS−1.15	Local	40.62	40.57	0.998
LCS−1.5	Local	89.84	89.29	0.993
LCS−2.5	Local	409.05	408.8	0.999
LCS-S220	Local	89.84	89.1	0.991
LCS-S350	Local	89.84	89.25	0.993
LCS-SWS−1.15	Distortional	138.71	131.35	0.946
LCS-DWS−1.15	Distortional	142.40	126.42	0.888
LCS-OWS−1.15	Distortional	154.27	151.94	0.984
LCS-SWS−1.5	Distortional	221.44	228.32	1.031
LCS-DWS−1.5	Distortional	226.37	219.05	0.967
LCS-OWS−1.5	Distortional	273.45	264.29	0.966
LCS-SWS−2.5	Distortional	650.65	665.97	1.02
LCS-DWS−2.5	Distortional	636.99	638.16	1.001
LCS-OWS−2.5	Distortional	762.63	762.78	1.00
B-B-LCS−1.15	Local	80.76	79.86	0.988
B-B-SWS−1.15	Distortional	232.19	262.7	1.131
B-B-DWS−1.15	Distortional	262.14	252.83	0.964
B-B-OWS−1.15	Distortional	283.94	303.88	1.07
B-B-LCS−1.5	Local	178.83	178.41	0.997
B-B-SWS−1.5	Distortional	375.93	458.39	1.219
B-B-DWS−1.5	Distortional	420.22	438.10	1.042
B-B-OWS−1.5	Distortional	529.85	528.96	0.998
B-B-LCS−2.5	Local	817.52	817.6	1.005
B-B-SWS−2.5	Distortional	1194	1331.94	1.115
B-B-DWS−2.5	Distortional	1275.36	1276.33	1.001
B-B-OWS−2.5	Distortional	1421.83	1525.47	1.072

exceeding 2 mm, demonstrating the accuracy of model's ability to capture the load-deformation behaviour for both stud configurations at room temperature. Lastly, the predominant failure mode observed in the FE model was web local buckling for both studs. This failure mode was consistent with those obtained from the aforementioned studies, as illustrated in Fig. 11.

5.2. Validation of thermal EF model under fire exposure

The thermal validation was also conducted for both single LCS and built-up I-shaped stud models, focusing initially on one-sided fire exposure. The single LCS thermal model was validated against the experimental study carried-out by Kolarkar [7], while the I-shaped stud model was validated according to the fire test established by Vy et al. [28]. These experimental studies followed standard fire testing procedures, including AS 1530.4, establishing criteria for structural integrity and flame spread prevention. This means that the fire testing setup primarily relied on radiation and convection heating to avoid any localized flame impingement and ensure a more uniform temperature distribution across the wall surface. The fire exposure was applied on one side of the plasterboard, and the maximum time-temperature progression was extracted at same thermocouples (TCs) locations, specifically, at the mid-height Hot Flange (HF) and Cold Flange (CF). According to Fig. 12 the maximum time-temperature progression predicted from the FEA models at each location showed a slight discrepancy with those produced by the TCs from the fire tests. A quantitative error analysis was conducted to assess the accuracy of developed thermal models in predicting time-temperature progression. For good validation, the obtained RMSE value should be smaller than the threshold of 100°C, as noted in EN1363–1 [52]. The RMSE was calculated for the temperature progression at each position, as presented in Table 4. It can be observed that the maximum RMSE values occurred at the HF for the single LCS and at the CF for the I-shaped stud, with values of 33.29°C and 41.57°C, respectively. Since these RMSE values are smaller than the threshold of 100°C, the thermal FEA model for both configurations has produced a reliable prediction of temperature evolution during one-sided fire exposure.

The thermal FEA model was validated under double-sided fire exposure, using the temperature rise recorded from the TCs during the fire test conducted by Inerhunwa et al. [37], as well as calibrated with the temperature evolution obtained from numerical study of Vy et al. [36]. According to the findings of these studies, the progression of the time-temperature at the mid-height of both stud flanges and the web exhibited nearly identical thermal behaviour. Therefore, for this validation and calibration, the time-temperature progression extracted from one of the stud flanges was used as a representative comparison for the overall thermal behaviour of the CFS stud wall model under double-sided fire exposure. Fig. 13 shows a comparison between the temperature progression predicted from ANSYS and the temperatures measured by TCs, as well as those obtained from FEA study of Vy et al. [36]. It can be seen that the predicted temperature follows a similar trend to those measured during the fire test, (validation), and those produced by the thermal FEA model of Vy et al. [36], (calibration), remaining consistent throughout the progression until failure. additionally, Table 4 shows a minor differences between these obtained temperatures, with RMSE values not exceeding 32 °C and 15 °C for the

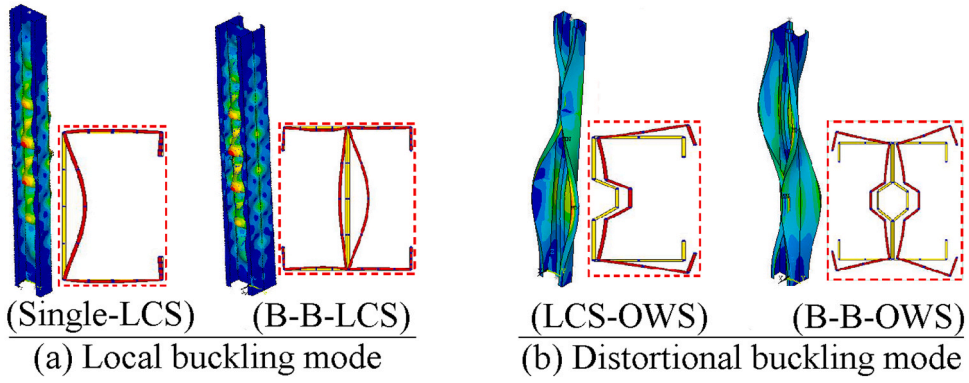

Fig. 9. Buckling modes for incorporating geometric imperfections in the reduced models.

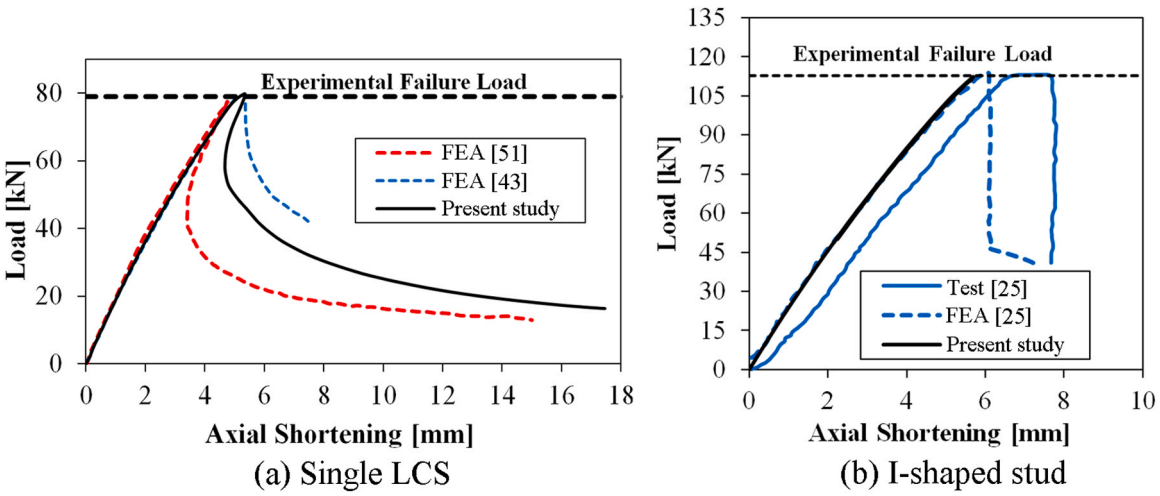

Fig. 10. Comparison of axial load-shortening curves predicted by ANSYS to those from the literature at room temperature.

Table 3
RMSE values for axial shortening of the developed structural models.

CFS configuration	Reference study	RMSE [mm]
Single LCS	Gunalan [51]	1.97
	Rokilan and Mahendran [43]	0.48
I-shaped Stud	Vy and Mahendran [25] (Test)	0.79
	Vy and Mahendran [25] (FEA)	0.06

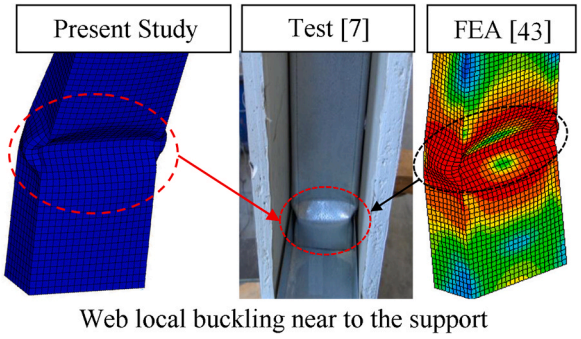

Fig. 11. Comparison of predicted failure mode to those from literature at room temperature.

fire test and the FEA of Vy et al. [36], respectively. These findings reflect a good approximation between the ANSYS simulation and the experimental and numerical studies, confirming the accuracy of the thermal FEA model in predicting the temperature evolution under double-sided fire exposure.

5.3. *Validation of structural FE model under fire exposure*

The process for validating the structural FEA model under fire exposure followed the same fire test procedure, applying an incremental load until reaching the designated load ratio. The temperature distribution were then incorporated in the structural FE model, with the applied load ratio maintained constant during the fire simulation until the model reached failure. It is important to note that the analysis considers only the heating phase following the ISO 834 fire curve, whereas real fire scenarios also include a cooling phase. The cooling phase can influence residual strength and the final failure state of the structure, which are not included in the current study. The validation for single LCS model under one-sided fire exposure was carried out by comparing the predicted load ratio-time curve to those obtained from the numerical study of Gunalan [51] and Rokilan and Mahendran [43], (Fig. 14 (a)). The predicted maximum temperature, failure time and failure mode were compared to the experimental study reported by Kolarkar [7]. It can be observed from Fig. 14 (a) that the comparison of the load ratio-time curve for the single LCS model indicates a good agreement between the three numerical studies. The predicted failure time from the present numerical model was 55 minutes, while the experimental failure time from Kolarkar [7] was recorded at 53 minutes, revealing a difference of only 3.6 %. Furthermore, as can be seen in Fig. 14 (b), both experimental and numerical models exhibited the same failure mode, characterised by global buckling accompanied by some web local buckling instabilities. The predicted maximum temperature was 631°C, while the measured maximum temperature was 607°C, resulting in a slight difference of 3.8 %. These results demonstrated the accuracy of the developed structural FE model in predicting the behaviour of LCS under one-sided fire exposure.

The structural I-shaped FEA model was validated under one-sided fire exposure against the fire test results and calibrated against the numerical study conducted by Vy et al. [28,29]. The validation and calibration were performed by comparing the axial shortening-time curves, failure times, and failure modes. As seen in Fig. 15 (a), the predicted axial shortening-time curve showed a close agreement with those obtained from both studies [28,29], demonstrating reasonable consistency throughout the fire exposure period. The predicted failure mode observed in the I-shaped stud was an interaction between local and global buckling, with a dominant influence of local buckling. This failure mode closely matched the one observed in the fire test, (Fig. 15 (b)). The developed I-shaped FEA model predicted a failure time of 127 minutes compared to the experimental failure time of 123 minutes, yielding a difference of 3.1 %. This close agreement further validates the model's ability to predict the structural performance of built-up I-shaped studs under one-sided fire exposure.

Due to the limited detailed data available from the fire test conducted by Inerhunwa et al. [37], the validation of the structural LCS model under both-sided fire exposure was carried out against the numerical study performed by Vy et al. [36]. The validation primarily focused on key performance indicators, including load-ratio time curves, failure time and critical temperature. As can be observed from Fig. 16, the load-ratio time curve predicted from ANSYS closely matched the corresponding curve obtained from the FEA of Vy et al. [36], with a failure time of 33 min, representing a small difference of 2.9 % compared to 34 minutes reported in the FEA study. Moreover, the predicted critical temperature was 642 °C, identical to that obtained from the FEA conducted by Vy et al. [36]. These comparisons between the obtained results from both numerical studies demonstrate that the

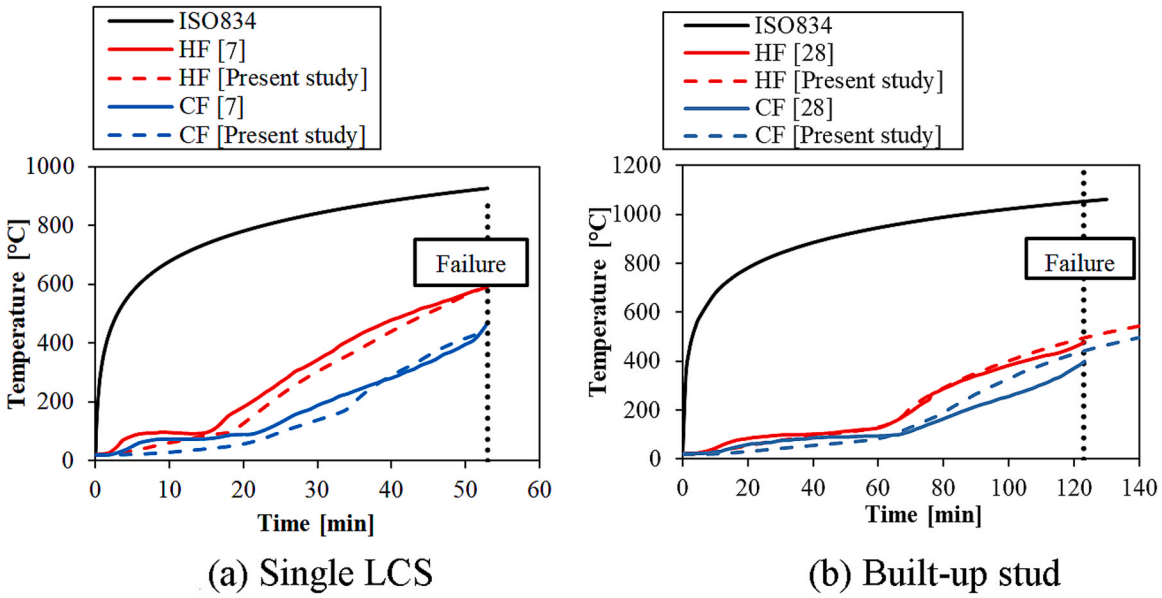

Fig. 12. Comparison of predicted and measured Time-Temperature progressions under one-sided fire exposure.

Table 4
RMSE values for temperature progression of the developed thermal models.

Fire scenario	CFS configuration	Reference study	TC position	RMSE [°C]
One-sided	Single LCS	Kolarkar [7]	HF	33.29
			CF	30.35
	B-B Stud	Vy et al. [28]	HF	18.16
			CF	41.57
Both-sided	Single LCS	Inerhunwa et al. [37]	Both Flanges	31.80
	Single LCS	Vy et al. [36]	Both Flanges	14.94

developed structural FEA model accurately predicts the behaviour of CFS model under both-sided fire exposure.

6. Parametric analysis

A total of 486 FEA CFS stud wall models were simulated using ANSYS Mechanical APDL [42] to investigate the thermal and structural performance of CFS stud walls under fire conditions. The analysis includes scenarios involving one-sided and double-sided fire exposure, accounting for various factors such as steel grade, thickness, web stiffeners and built-up I-shaped configurations.

6.1. Time-temperature progression

Fig. 17 presents the time-temperature curves for LCS with varying steel thicknesses, subjected to one-sided (#1) and double-sided (#2) fire exposure.

These curves were recorded at the mid-height HF and CF of the stud after 60 minutes of exposure to fire. A comparison between the temperatures progression of the reference stud with those of SWS and B-B-LCS under the two fire exposure scenarios is also provided in Fig. 17. The temperature across the stud surfaces obtained under one-sided fire exposure remains lower than under double-sided fire exposure. The comparison shows that the effect of steel thickness on temperature distribution is more pronounced under one-sided fire exposure, where thicker studs exhibit lower surface temperatures, while thinner studs experience higher surface temperatures. The results clearly demonstrate

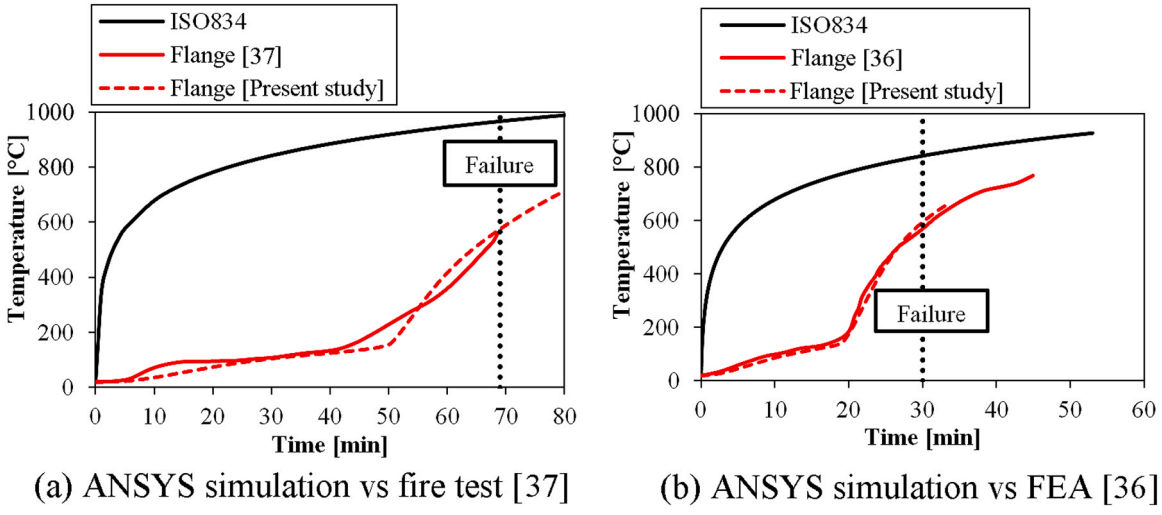

Fig. 13. Comparison of predicted temperature progression with those from literature under double-sided fire exposure.

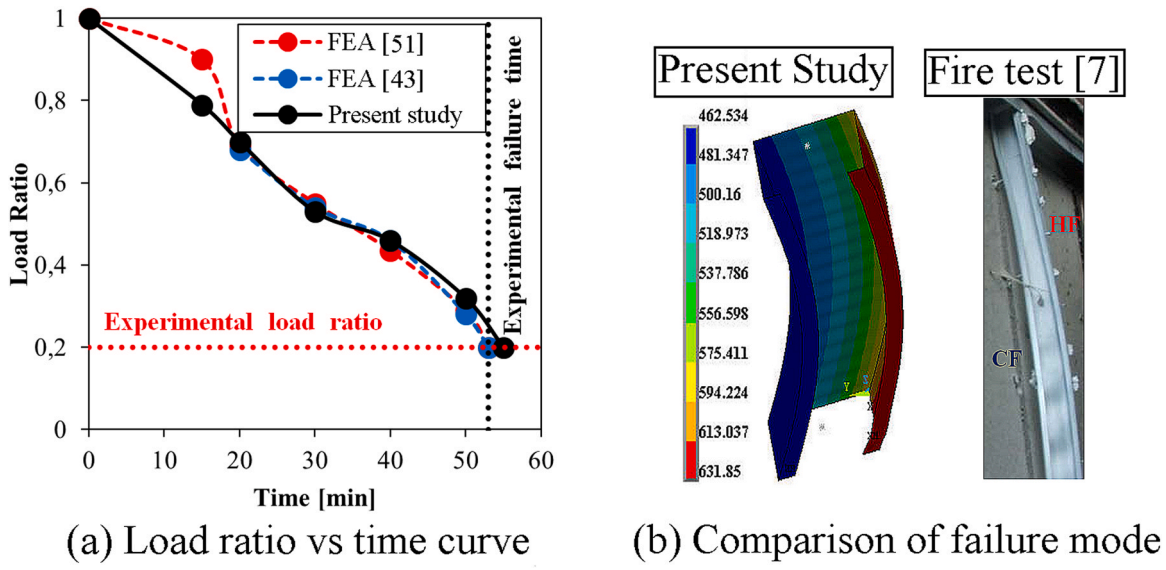

Fig. 14. Validation of LCS structural FE model under one-sided fire exposure.

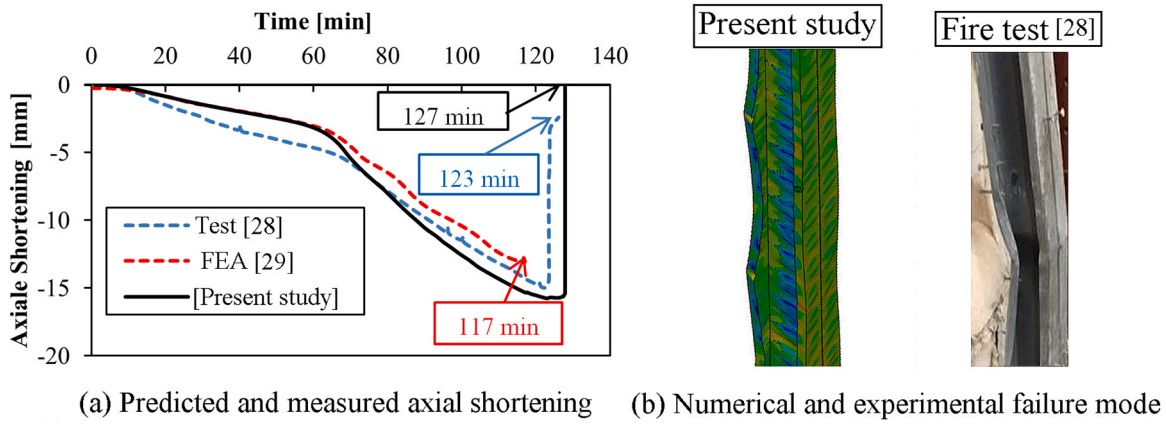

Fig. 15. Validation of I-shaped structural FE model under one-sided fire exposure.

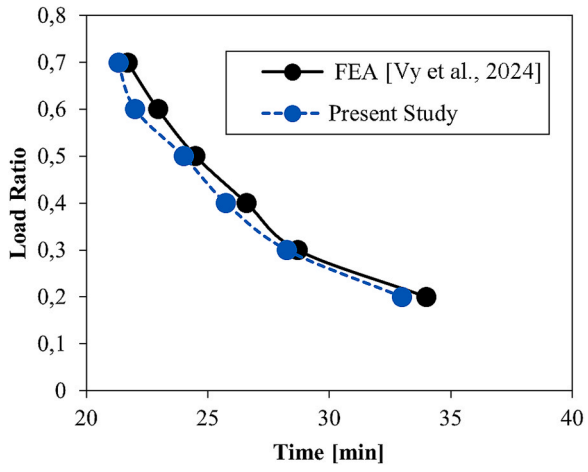

Fig. 16. Comparison of Load ratio-time curve under doubled-sided fire exposure.

that increasing steel thickness significantly reduces CFS surface temperatures. However, under double-sided fire exposure, the effect of steel thickness is less pronounced for the 1.15 mm and 1.5 mm studs, as they exhibit nearly identical temperature distributions. In contrast, the 2.5 mm thick stud results in a noticeably lower temperature distribution compared to the thinner studs. Moreover, a notable difference in temperature evolution between the two flanges was observed in one-sided fire exposure, where the HF experienced significantly higher temperatures than the CF. In contrast, the temperatures across both flanges under double-sided fire exposure, were more uniform. It is worth mentioning that the time-temperature curve for LCS-1.5 was applied to all studs with different steel grades in this study, as these studs have the same steel thickness and identical fire protection configuration. Also, it can be seen from Fig. 17 that the temperatures evolution of LCS-T1.5 are identical to those of LCS-SWS-1.5 and B-B-LCS-1.5 for both fire exposure scenarios. This same trend is observed for other stiffened and I-shaped studs, including DWS, OWS, B-B-SWS, B-B-DWS and B-B-OWS, suggesting that including stiffeners or doubling the studs has minimal influence on the CFS walls thermal response.

Several practical strategies can be employed to mitigate the impact of double-sided fire exposure on CFS walls by reducing the rate of temperature increase. One effective approach is incorporating high-performance insulation materials, such as Superwool, Rockwool or glass fibre sandwiched between external protective layers. This configuration significantly slows heat transfer and protects CFS surfaces from rapid temperature progression. Additionally, increasing the thickness or number of protective layers, (i.e. double or multiple layers of

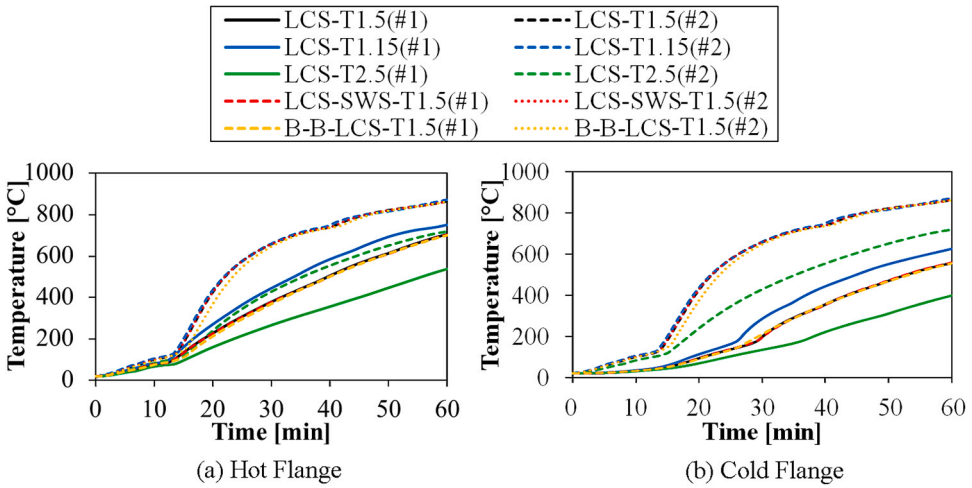

Fig. 17. Effect of steel thickness, web stiffeners and I-shaped configurations on temperature progression of LCS walls under one-sided (#1) and double-sided (#2) fire exposure.

plasterboards), improves the insulation fire resistance and delays temperature rise, thereby improving the fire resistance of the assembly.

6.2. Fire resistance

The fire resistance is determined based on the load ratio-time curve, which illustrates the structural capacity of the stud wall to support varying load levels (ranging from 20 % to 80 %) relative to its load-bearing capacity at room temperature. In this study, a load ratio of 0.2 is considered as failure reference for all CFS models for the two fire exposure scenarios.

6.2.1. Effect of steel thickness and grade

Fig. 18 presents a comparison of the fire resistance for LCS models with varying steel thickness and grade under one-sided and double-sided fire exposure scenarios. From Fig. 18 (a), it can be observed that the LCS-T1.15 and LCS-T1.5 models reached failure at 48 and 56 minutes, respectively, when exposed to fire from one side, while the LCS-T2.5 model did not fail within the 60 minute exposure period. This indicates that increasing the thickness of steel enhances the fire resistance (R) when exposed to fire from one side. Conversely, in the case of double-sided fire exposure, LCS-T1.15 and LCS-T1.5 both reached failure at 28 minutes, with the LCS-T2.5 model only showing a slight improvement, failing after 30 minutes. The switch from one-sided to double-sided fire exposure resulted in more than a 41 % and 50 % reduction in fire resistance (R) for LCS-T1.15 and LCS-T1.5, respectively. It can be seen from the same figure that the steel grade of S220, S280 or S350 achieved the same failure time when considering specific load ratios. However, as illustrated in Fig. 18 (b), increasing the steel grade leads to higher load-bearing capacity at room temperature, which subsequently results in improved fire resistance for both fire exposure cases. For example, an applied load of 40 kN results failure times of 26, 32 and 36 min for S220, S280 and S350, respectively, under one-sided fire exposure. Also, it can be seen that the load bearing capacity of CFS studs decreases progressively over time as the fire exposure continues due to the deterioration in the mechanical properties. The degradation rate is significantly more rapid for models exposed to double-sided fire than one-sided fire exposure. This is because the temperature distribution across the stud surfaces becomes nearly uniform. Fig. 19 (a) illustrates the deformed shapes and Von Mises stress distribution of LCS-T1.5 models with steel grades of S280 and S350, when subjected to one-sided fire exposure. The failure mode for both steel grades remains consistent, exhibiting an interaction of local/distortional and some global buckling instabilities, caused due to the significant temperature

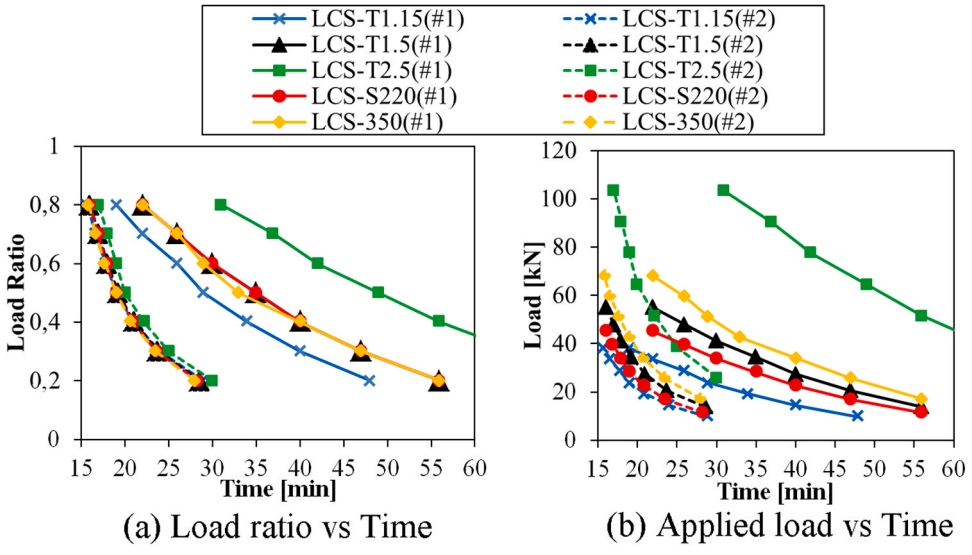

Fig. 18. Effect of steel thickness and grade on the structural performance of single LCS walls under one-sided (#1) and double-sided (#2) fire exposure.

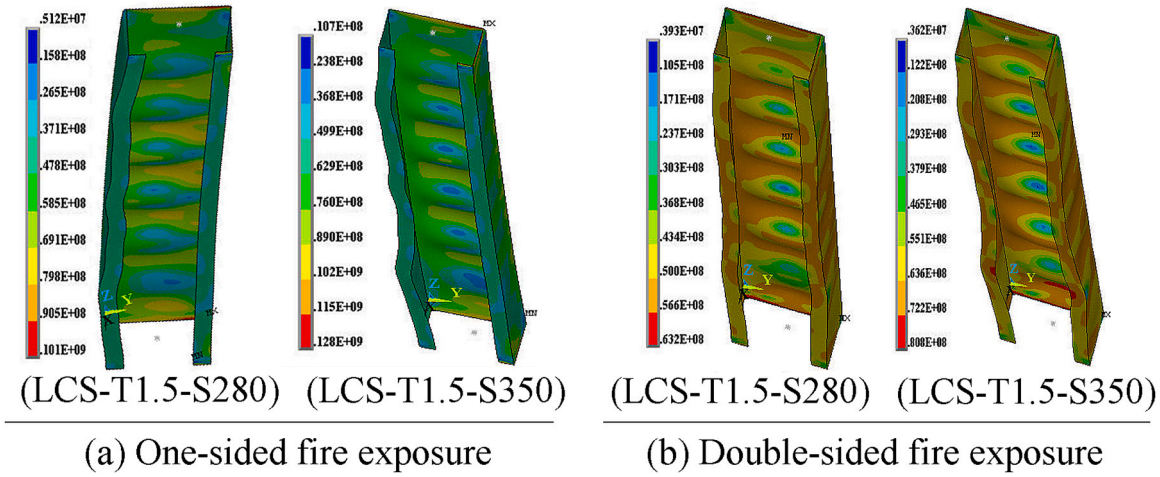

Fig. 19. Failure modes (scaled by a factor of 5) of LCS-T1.5 with different steel grade.

difference between the HF and CF. Because of this uneven temperature distribution, the HF experiences more significant thermal expansion, causing the stud to bend toward the fire-exposed side. The dominant failure mode obtained under double-sided fire exposure was local/distortional buckling with global buckling is less pronounced compared to the one-sided fire exposure, (Fig. 19 (b)), as the thermal expansion is more evenly distributed between the two flanges. All LCS models, regardless of their thickness and grade, exhibit the same failure mode for both cases.

6.2.2. Effect of web stiffeners and built-up I-shaped stud configurations

It can be observed from Fig. 20 that the inclusion of web stiffeners, such as SWS, DWS, and OWS, has only a slight effect on the structural fire behaviour of CFS stud walls. At ambient temperature, the presence of web stiffeners results in a marginal increase in load-bearing capacity, with the highest improvement of 7.5 % observed for the 2.5 mm thick OWS-stiffened stud. However, these configurations exhibit minimal variation in failure time, within a range of only a few minutes from unstiffened LCS for different steel thicknesses including 1.15 mm, (Fig. 20 (a)), 1.5 mm, (Fig. 20 (b)), and 2.5 mm (Fig. 20 (c)). The rate of degradation in load-bearing capacity remains similar across all configurations under both one-sided and double-sided fire exposure, confirming that web stiffeners do not significantly improve the CFS fire resistance performance. Arranging stiffened and unstiffened studs in a built-up I-shaped configuration significantly increases the load-bearing capacity at room temperature, nearly doubling it compared to single studs. The improvement rate in load-bearing capacity observed for a single stud with web stiffeners is approximately the same as that achieved when incorporating web stiffeners in the built-up configuration. This enhanced load-bearing capacity also leads to improved fire resistance for both cases. Although the built-up I-shaped models exhibit failure times identical to those of single studs when subjected to the same applied load ratios, the increased load-bearing capacity at room temperature contributes to enhance the fire resistance performance. For instance, as shown in Fig. 20 (b), an applied load of 40 kN results in failure times of 30 minutes and 47 minutes for single LCS-1.5 and B-B-LCS-1.5, respectively, under one-sided fire exposure. These failure times were decreased to 18 minutes and 25 minutes under double-sided fire exposure for the same configurations.

The failure modes and Von Mises stress distribution of B-B-LCS, LCS-SWS and B-B-SWS with thickness of 1.5 mm under both fire exposure scenarios are shown in Fig. 21. The failure mode for B-B-LCS is identical to the deformed shape of the single stud (LCS-T1.5), regardless of the fire exposure scenario. As shown in Fig. 21 (a), the failure mode for both LCS-SWS and B-B-SWS models under one-sided fire exposure was dominated purely by distortional buckling, without any contribution from global buckling instability. Including stiffeners on the stud web leads to stiffening the web against local buckling, and reduces global instability of the overall stud element. The same failure mode remained the primary failure mechanism under double-sided fire exposure, as illustrated in Fig. 21 (b), since the uniform temperature distribution across the stud surfaces, as well as the effect of web stiffeners reduce the occurrence of global buckling. The same modes were occurred for the other stiffened and built-up stud models.

Other innovative reinforcement techniques can further improve the fire resistance of CFS walls, such as built-up I-shaped studs with hollow flanges and built-up nested studs. Built-up I-shaped studs with hollow flanges may significantly enhance the load-bearing capacity. However, their manufacturing process is more complex, time-consuming and costly compared to conventional I-shaped studs, making them less practical for widespread use. Alternatively, built-up nested studs, as investigated by Vy et al. [29]., demonstrated similar performance to I-shaped studs. While nested studs may provide advantages in case of using fire insulation materials, conventional I-shaped studs have open cross-sections which offer greater flexibility and suitable solution for uninsulated CFS walls.

7. Novel approach for the prediction of the maximum temperature and fire resistance for CFS walls

The maximum temperature (T_{max}) is defined as the temperature recorded at the stud HF at failure for each applied load ratio. This temperature indicates the structural limit where the CFS stud walls can no longer sustain the applied load. If one knows the value of the maximum temperature, the degree of utilisation can be related with the value of the load ratio, (Eq. (3)), and the results can be compared.

$$Load\ ratio = \mu_0 \bullet \frac{N_{b,fi,0,Rd}}{N_{b,Rd}} \text{With} \mu_0 = \frac{N_{fi,Ed}}{N_{b,fi,0,Rd}} \tag{3}$$

Where: $N_{b,rd}$ is the design buckling resistance at room temperature, $N_{fi,Ed}$ is the design value of axial compression load in the fire situation; $N_{b,fi,0,rd}$ is the design buckling resistance at (t = 0) of a compression member.

Fig. 22 presents a comparison of the load ratio versus the maximum temperatures obtained from the numerical simulations with those predicted by the EC3 for both fire exposure scenarios. It can be observed from Fig. 22 that all models reached nearly identical maximum temperatures when subjected to the same load ratio and fire exposure scenario. This uniformity highlights the direct relationship between the applied load and the temperature at which failure occurs, suggesting that fire resistance is predominantly influenced by the load ratio. Also, Fig. 22 illustrates that the prediction from EN1993–1–2 [22] is too

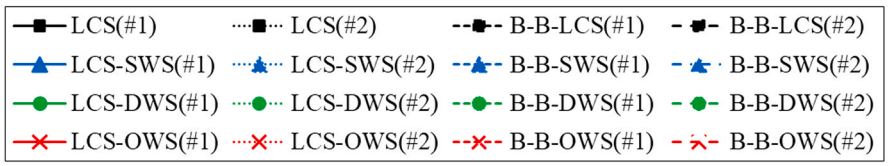

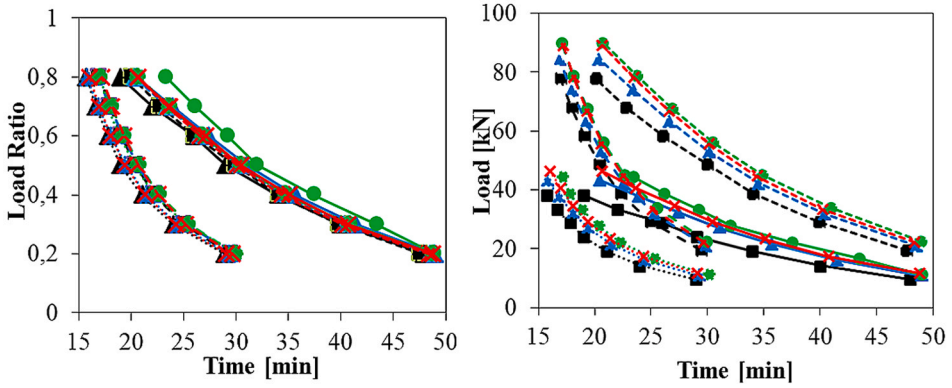

(Load ratio vs Time) (Applied load vs Time)

(a) CFS thickness-1.15 mm-

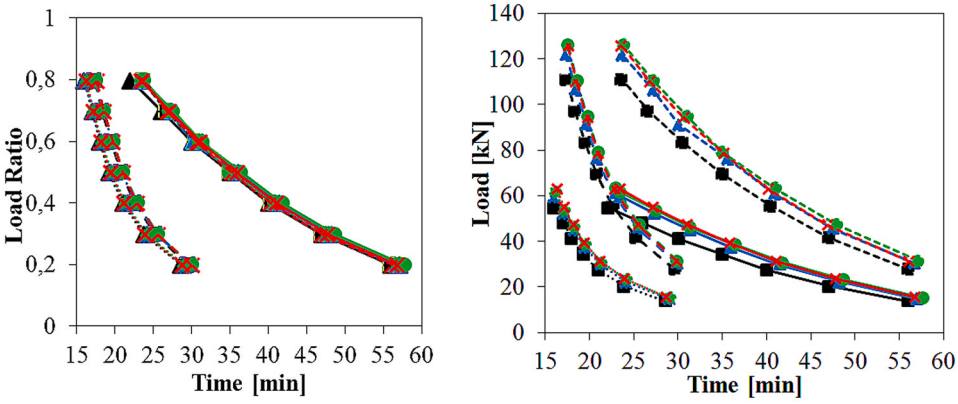

(Load ratio vs Time) (Applied load vs Time)

(b) CFS thickness-1.5 mm-

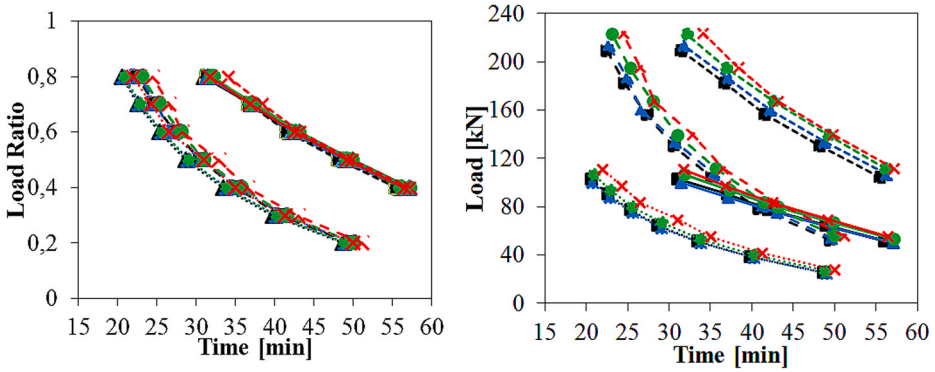

(Load ratio vs Time) (Applied load vs Time)

(c) CFS thickness-2.5 mm-

Fig. 20. Effect of web stiffeners and I-shaped stud configurations on the structural performance of LCS stud walls under one-sided (#1) and double-sided (#2) fire exposure.

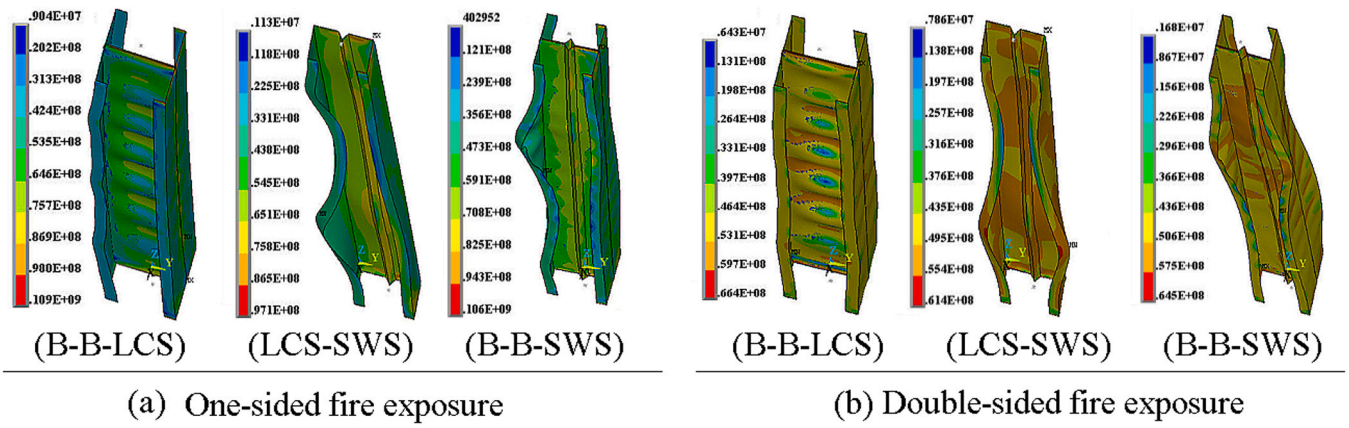

Fig. 21. Failure modes (scaled by a factor of 5) of CFS with thickness of 1.5 mm under fire.

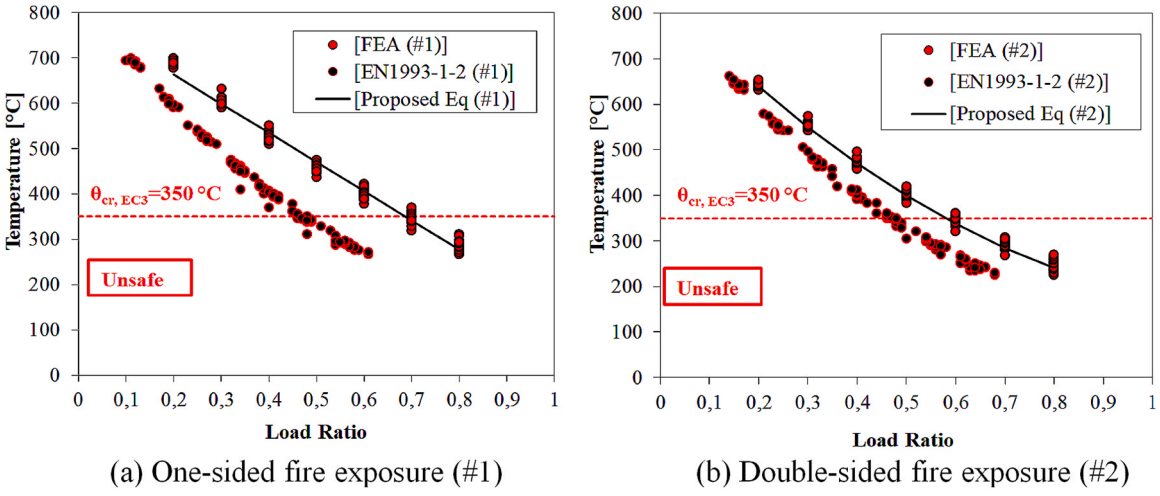

Fig. 22. Comparison of the maximum temperature of FE models and EC3 analytical method.

conservative compared to those from the simulated models for both cases. The discrepancy between the two studies becomes more apparent at higher load levels, especially in the case of one-sided fire exposure. Furthermore, the results highlight a safety concern in using the temperature limit provided by EN1993–1–2 [22], which states that the fire resistance can be verified if the temperature of CFS surfaces remains below 350°C. This limit is generally over conservative for most cases, proving unsafe for load levels exceeding 60 % under one-sided fire exposure and 50 % under double-sided fire exposure. At these higher load levels, failure occurs at temperatures below the 350°C threshold, indicating that the simplified method in EC3 may underestimate the risk of early failure. Building upon these results, Eq. (4) and Eq. (5) have been developed based on load ratio (LR), to estimate the maximum temperature of CFS stud walls at failure under one-sided and both-sided fire exposure, respectively. These proposals may ensure a high safety level for structural fire resistance assessments for CFS stud walls.

$$(1):\ T_{\max}[^{\circ}C] = (-643.23 \times LR) + 791.78; \quad 0.2 \le LR \le 0.8 \tag{4}$$

$$(2):\ T_{\max}[^{\circ}C] = \left(442.9 \times LR^2\right) - 1107 \times LR + 842.5; \quad 0.2 \le LR \le 0.8 \tag{5}$$

Additionally, new equations are proposed for predicting idealised time-temperature curves for the maximum temperature progression in stud HF for different time intervals, up to 60 minutes of fire exposure, specifically for the three different CFS thicknesses used in this study. These equations are derived from the numerical thermal results, and serve as a key factor in determining the fire resistance based on the maximum temperature proposal. The idealised time-temperature curves for the three steel thicknesses, (Fig. 23), can be determined using Eqs. (6–11) and Eqs. (12–15), for one-sided and both sided fire exposure, respectively.

One-sided fire exposure (#1):

$$\text{T1.15 (\#1)}: T_{HF}[^{\circ}C] = -0.049t^3 + 0.941t^2 + 1.866t + 19.25; \quad 0 \le t\ [\text{min}] < 13 \tag{6}$$

$$T_{HF}[^{\circ}C] = -0.19t^2 + 27.41t - 204.9; \quad 13 \le t\ [\text{min}] \le 60 \tag{7}$$

$$\text{T1.5 (\#1)}: T_{HF}[^{\circ}C] = 6t + 14.77; \quad 0 \le t\ [\text{min}] < 13 \tag{8}$$

$$T_{HF}[^{\circ}C] = -0.109t^2 + 20.73t - 146.5; \quad 13 \le t\ [\text{min}] \le 60 \tag{9}$$

$$\text{T2.5 (\#1)}: T_{HF}[^{\circ}C] = 4.95t + 14.65; \quad 0 \le t\ [\text{min}] < 15 \tag{10}$$

$$T_{HF}[^{\circ}C] = -0.029t^2 + 11.72t - 62.79; \quad 15 \le t\ [\text{min}] \le 60 \tag{11}$$

Both-sided fire exposure (#2):

$$\text{T1.15 and T1.5 (\#2)}: T_{HF}[^{\circ}C] = 8.66t + 13.77; \quad 0 \le t\ [\text{min}] < 14 \tag{12}$$

$$T_{HF}[^{\circ}C] = 0.014t3 - 0.1947t^2 + 96.95t - 850.2; 14 \quad \le t[\text{Min}] \le 60 \tag{13}$$

$$\text{T2.5 (\#2)}: T_{HF}[^{\circ}C] = 6.888t + 11.9; \quad 0 \le t\ [\text{min}] < 15 \tag{14}$$

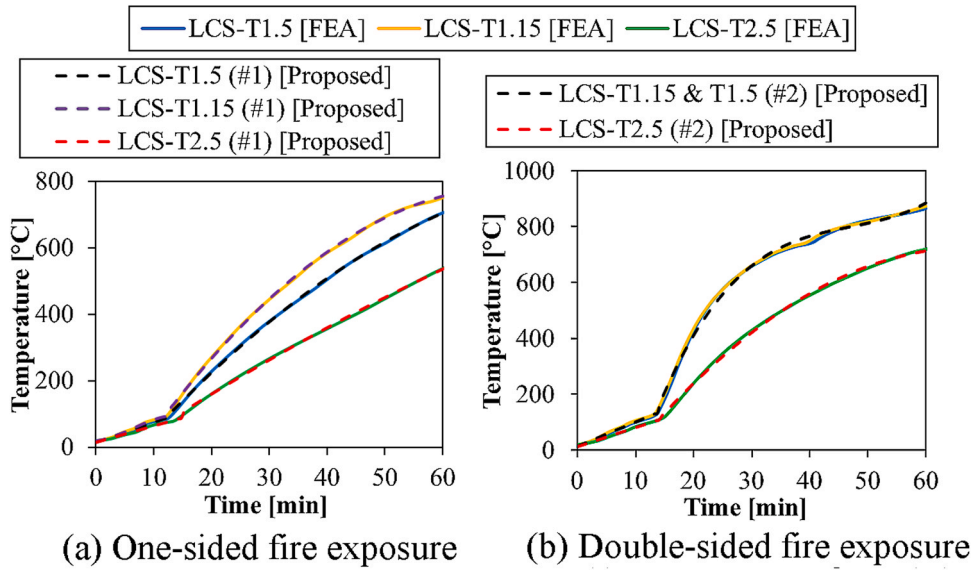

Fig. 23. Idealised Time-Temperature curves for LCS (T1.15, T1.5 and T2.5).

$$T_{HF}[^{\circ}C] = -0.211t^2 + 28.71t - 250.5; \quad 15 \leq t\,[\text{min}] \leq 60 \qquad (15)$$

The goodness-of-fit between the fire resistance predicted from FE models and those determined using the proposed approach which is based on the proposed maximum temperature equations and idealised time-temperature curves was evaluated under one-sided and both-sided fire exposure. As illustrated in Fig. 24, the comparison was made by analysing the R^2 values for a polynomial fit, which reflects the accuracy of the proposed method in predicting the fire resistance. It can be observed from Fig. 24 that most of the data points fall within the trend-line zone, staying within the error limit lines of + /-10 %, which suggests that the proposed approach is highly reliable and effective for predicting the critical temperature and fire resistance for both fire exposure scenarios. Additionally, the R^2 value was found to be 0.984 for one-sided fire exposure, (Fig. 24 (a)), while it reached 0.976 for both-sided fire exposure, (Fig. 24 (b)). These high R^2 values indicate a strong correlation between the FE model predictions and the failure time values derived from the proposed approach.

The proposed method is highly dependent on the idealised time-temperature equations developed in this study, which are tailored specifically to the protection configurations and steel thicknesses used in this investigation. As a result, the equations may not apply to CFS walls with different protection systems (i.e insulated walls) or steel thicknesses beyond those used in this study.

8. Validation of proposed formulas against real-world fire test

To validate the proposed formula for one sided fire exposure, (Eq. 4), against real-world fire conditions, comparisons were made with experimental fire tests conducted by Ariyanayagam and Mahendran [53] based on Broadgate Fire Dynamics (BFD) curve. Two types of uninsulated LSF walls including, LSF2, (double layers of plasterboard), and LSF4, (single layer of plasterboard), are considered in the validation. Table 5 presents a comparison of the maximum temperature predicted

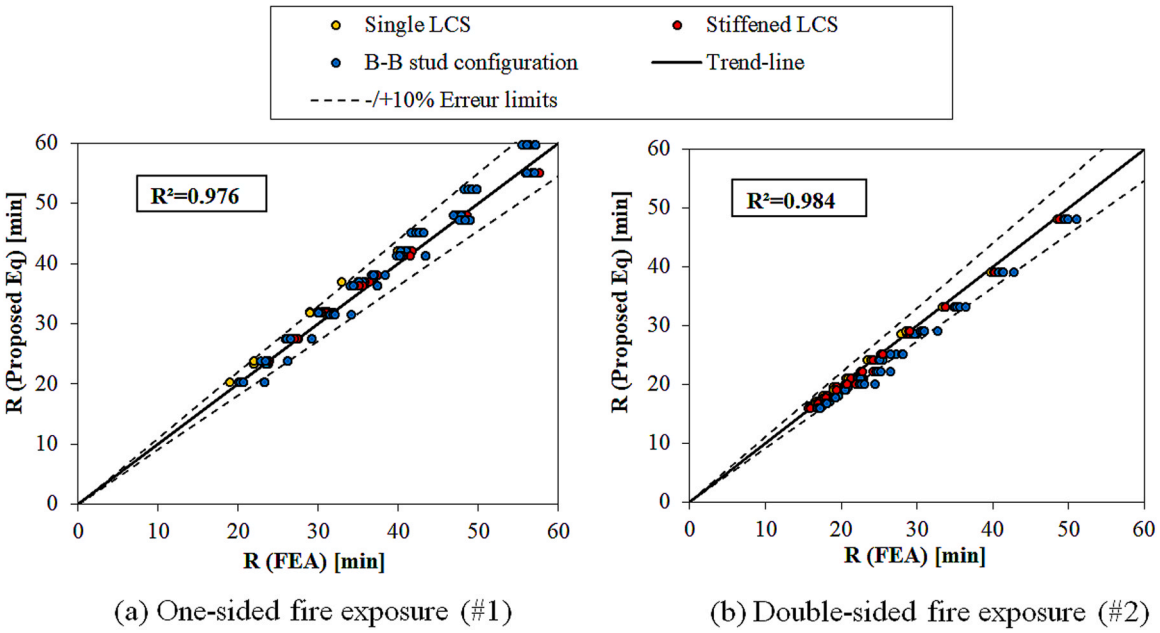

Fig. 24. Comparison of Fire Resistance (R) predicted by FEA and the proposed approach.

by the proposed formula with those obtained from fire tests. The results indicate a slight difference between the predicted and experimental temperatures, with deviations of 2.7 % and 4.9 % for LSF 2 and LSF 4, respectively, demonstrating strong agreement between the proposed formula and experimental data for one-sided fire exposure.

9. Conclusions

A comprehensive parametric analysis was conducted to evaluate the performance of CFS stud walls subjected to axial compression load under two fire exposure scenarios, including one-sided and double-sided fire exposure. Several parameters were varied, including steel thickness and grade, the presence of different types of web stiffeners and built-up I-shaped stud configurations. Several load ratios (0.2–0.8) were applied to determine the maximum temperature and the fire resistance. Following are the important conclusions from this study:

- The maximum temperature progression remains unaffected by the presence of web stiffeners or doubling studs in built-up I-shaped configurations.
- Increasing the steel thickness significantly reduces temperature progression and enhances the fire resistance, while its effect is less pronounced for CFS thicknesses of 1.15 mm and 1.5 mm in the case of double-sided fire exposure.
- Steel grade and built-up I-shaped configurations enhance the load-bearing capacity at room temperature, thereby improving fire resistance under both fire exposure scenarios.
- Web stiffener configurations have only a slight effect on fire resistance performance.
- Switching from one-sided to both-sided fire exposure for LCS-T1.15 and LCS-T1.5 results in a 41 % and 50 % reduction in fire resistance, respectively.
- The load ratio versus the maximum temperatures predicted by EN1993–1–2 [22] were found to be conservative when compared to the numerical simulation results.
- The temperature limit of 350°C recommended by EN1993–1–2 [22] to verify fire resistance proves to be unsafe for load levels exceeding 60 % under one-sided fire exposure and 50 % under double-sided fire exposure.
- New formulas, based on load ratio have been proposed to predict the maximum temperature at failure for CFS walls under one-sided and doubled-sided fire exposure.
- New approach has been developed to determine the fire resistance of CFS walls, using the proposed idealised time-temperature equations as well as the proposed formulas for the maximum temperature.
- The developed approach offered reliable predictions for different stud configuration and exhibited high accuracy, with R^2 values of 0.976 and 0.984 for one-sided and double-sided fire exposure, respectively.

The dimensions of the specimen affect the failure modes of the cladding system (gypsum), affecting the overall temperature field in the model, introducing different crack patterns, different ablation modes and opening joints when available. These events may introduce a small modification in the fire resistance by insulation (I) of reduced-scale specimens in comparison to full-scale specimens. The dimension of the specimens also influences the expected structural failure modes of the CFS stud walls, in particular for the reduced-scale specimen, reducing the risk of some global failure modes. The reduced dimension of the specimens is expected to increase the maximum temperature of the LSF wall, increasing the fire resistance by stability (R), as already verified by Piloto et al. [21].

The proposed approach provides structural fire engineers with formulas to determine the maximum temperature of CFS wall under both, one-sided and double-sided fire exposure. Therefore, the estimation of the fire resistance for these cases would be more accurate for the design of safer CFS stud walls under fire.

Future trends in the fire resistance of CFS stud walls should consider the possibility of determining the fire resistance based on a simplified additive component procedure in terms of the fire resistance by insulation. This simplified method may be based on the separating function method.

Table 5
Maximum temperature for one-sided exposure: proposed formula vs BFD.

Specimen	Fire action	Load ratio	$T_{max\ (Eq.4)}$ [°C]	$T_{max\ (Test)}$ [°C]	Difference [%]
LSF 2	BFD	0.2	663	645	2.7
LSF 4	BFD	0.2	663	630	4.9

CRediT authorship contribution statement

Piloto Paulo A. G.: Writing – review & editing, Supervision, Conceptualization. **Jiang Liming:** Writing – review & editing, Supervision, Conceptualization. **Yessad Ouissam:** Writing – review & editing. **Menadi Belkacem:** Writing – review & editing, Supervision, Conceptualization. **Lamri Belkacem:** Writing – review & editing, Supervision, Conceptualization. **Hassoune Mohammed:** Writing – review & editing, Writing – original draft, Validation, Methodology, Investigation, Conceptualization. **Kada Abdelhak:** Writing – review & editing, Supervision, Conceptualization.

Declaration of Competing Interest

The authors declare that they have no known competing financial interests or personal relationships that could have appeared to influence the work reported in this paper.

Data availability

Data will be made available on request.

References

[1] Rouaz I, Bouzid H. Numerical evaluation of shear strength of CFS shear wall panel with OSB sheathing. Structures 2023;57:105330. https://doi.org/10.1016/j.istruc.2023.105330.
[2] Thirunavukkarasu K, Kanthasamy E, Gatheeshgar P, Poologanathan K, Rajanayagam H, Suntharalingam T, Dissanayake M. Sustainable performance of a modular building system made of built-up cold-formed steel beams. Buildings 2021;11:460. https://doi.org/10.3390/buildings11100460.
[3] Cashell KA, Malaska M, Khan M, Alanen M, Mela K. Experimental and numerical analysis of stainless steel cellular beams in fire. Fire Saf J 2021;121:103277. https://doi.org/10.1016/j.firesaf.2021.103277.
[4] Vlasov, V.Z., Thin-Walled Elastic Beams. Published for the National Science Foundation, Washington D.C. and the Department of Commerce, USA. (1961).
[5] Kada A, Lamri B. Numerical analysis of non-restrained long-span steel beams at high temperatures due to fire. Asian J Civ Eng 2019;20:261–7. https://doi.org/10.1007/s42107-018-0103-7.
[6] Qiu J, Jiang L. Development of modular and reusable AI models for fast predicting fire behaviour of steel columns in structural systems. Eng Struct 2023;297:116994. https://doi.org/10.1016/j.engstruct.2023.116994.
[7] Kolarkar, P.N., Structural and thermal performance of cold-formed steel stud wall systems under fire conditions. (PhD Thesis), School of urban development, Queensland University of Technology, Australia, 2010.
[8] Gunalan S, Kolarkar P, Mahendran M. Experimental study of load bearing cold-formed steel wall systems under fire conditions. Thin Walled Struct 2013;65:72–92. https://doi.org/10.1016/j.tws.2013.01.005.
[9] Piloto, P., Light steel framed walls made with composite panels under fire conditions. Proceedings of 6th Conference on Urban Fire Safety and 1st Civil Protection Conference, Universidade de Coimbra- Portugal 2018, pp. 103-123.
[10] Steau E, Mahendran M, Poologanathan K. Experimental study of fire resistant board configurations under standard fire conditions. Fire Saf J 2020;116:103153. https://doi.org/10.1016/j.firesaf.2020.103153.
[11] Liu K, Chen W, Ye J, Gao L, Jiang J. Experimental investigation of the quantified influence of gypsum plasterboard joints on the fire performance of cold-formed steel walls. Structures 2023;49:312–31. https://doi.org/10.1016/j.istruc.2023.01.127.

[12] Liu K, Chen W, Ye J, Jiang J, Fang Z, Lim JB. Fire performance enhancement of cold-formed steel walls: experimental and numerical study. Eng Struct 2024;314:118419. https://doi.org/10.1016/j.engstruct.2024.118419.
[13] Ranawaka T, Mahendran M. Numerical modelling of light gauge cold-formed steel compression members subjected to distortional buckling at elevated temperatures. Thin Walled Struct 2010;48:334–44. https://doi.org/10.1016/j.tws.2009.11.004.
[14] Piloto, P., Khetata, M., and Gavilán, A.B., Fire resistance of non-loadbearing LSF walls. Proceedings of 2nd Conference on Testing and Experimentations in Civil Engineering, Porto, Portugal, 2019, pp. 429-440.
[15] Khetata SM, Piloto PA, Gavilán AB. Fire resistance of composite non-load bearing light steel framing walls. J Fire Sci 2020;38:136–55. https://doi.org/10.1177/0734904119900931.
[16] Tao Y, Mahendran M, Ariyanayagam A. Numerical study of LSF walls made of cold-formed steel hollow section studs in fire. Thin Walled Struct 2021;167:108181. https://doi.org/10.1016/j.tws.2021.108181.
[17] Hassoune M, Kada A, Menadi B, Lamri B. Numerical thermal performance analysis of light steel insulated walls under fire. Građevinski Mater i Konstr=Build Mater Struct 2023;66:43–54. https://doi.org/10.5937/GRMK2301043H.
[18] Hassoune, M., Kada, A., Menadi, B., Lamri, B., Bouchair, A., and Jiang, L., Influence of Double Protection Layers on the Fire Resistance of Load-Bearing LSF Wall Panels. Proceedings of The 7th International Conference series on Geotechnics, Civil Engineering and Structures, (CIGOS 2024), Ho Chi Minh City, Vietnam, 2024, pp. 451-459. https://doi.org/10.1007/978-981-97-1972-3_49.
[19] Xing Y, Zhao O, Wang W. Testing, modelling and analysis of full-scale cold-formed steel center-sheathed shear walls in fire. Eng Struct 2023;284:115970. https://doi.org/10.1016/j.engstruct.2023.115970.
[20] Torres L, Couto C, Real PV, Piloto P. Numerical study of the fire behaviour of external walls in light steel framing. Fire Saf J 2023;141:103946. https://doi.org/10.1016/j.firesaf.2023.103946.
[21] Piloto PA, Khetata MS, Ramos-Gavilán AB. Analysis of the critical temperature on load bearing LSF walls under fire. Eng Struct 2022;270:114858. https://doi.org/10.1016/j.engstruct.2022.114858.
[22] EN1993-1-2, Eurocode 3: Design of steel structures - Part 1-2: General rules - Structural fire design [Authority: The European Union Per Regulation 305/2011, Directive 98/34/EC, Directive 2004/18/EC]. (2005), 78.
[23] Kechidi S, Fratamico DC, Schafer BW, Castro JM, Bourahla N. Simulation of screw connected built-up cold-formed steel back-to-back lipped channels under axial compression. Eng Struct 2020;206:110109. https://doi.org/10.1016/j.engstruct.2019.110109.
[24] Fratamico DC, Torabian S, Zhao X, Rasmussen KJ, Schafer BW. Experimental study on the composite action in sheathed and bare built-up cold-formed steel columns. Thin Walled Struct 2018;127:290–305. https://doi.org/10.1016/j.tws.2018.02.002.
[25] Vy ST, Mahendran M. Design of built-up back-to-back CFS channel compression members sheathed with gypsum plasterboards. J Constr Steel Res 2022;199:107607. https://doi.org/10.1016/j.jcsr.2022.107607.
[26] Vy ST, Mahendran M. Design of sheathed built-up nested CFS channel studs in load-bearing LSF walls. Thin Walled Struct 2023;182:110197. https://doi.org/10.1016/j.tws.2022.110197.
[27] Hassoune, M., Kada, A., Menadi, B., and Lamri, B., Numerical study of the response of cold-formed steel sections used in wall panels when subjected to fire. Proceedings of 12th International Conference on Structures in Fire (SIF2022), Hong kong, 2022, pp. 1004-1014. https://doi.org/10.6084/m9.figshare.22215775.
[28] Vy ST, Mahendran M, Steau E, Ariyanayagam A. Full-scale tests of load-bearing LSF walls made of built-up CFS channel sections under fire conditions. Thin Walled Struct 2023;187:110763. https://doi.org/10.1016/j.tws.2023.110763.
[29] Vy ST, Mahendran M, Ariyanayagam A. Numerical modelling and investigation of CFS built-up stud walls in fire. Fire Saf J 2024;144:104102. https://doi.org/10.1016/j.firesaf.2024.104102.
[30] Sam VS, Marak GWK, Nammalvar A, Andrushia D, Gurupatham BGA, Roy K. Investigation on flexural behavior of galvanized cold-formed steel beams exposed to fire with different stiffener configurations. Fire 2024;7:318. https://doi.org/10.3390/fire7090318.
[31] Sam VS, Nammalvar A, Andrushia D, Gurupatham BGA, Roy K. Flexural behavior of galvanized iron based cold-formed steel back-to-back built-up beams at elevated temperatures. Buildings 2024;14:2456. https://doi.org/10.3390/buildings14082456.
[32] Rusthi M, Ariyanayagam AD, Mahendran M. Fire design of LSF wall systems made of web-stiffened lipped channel studs. Thin Walled Struct 2018;127:588–603. https://doi.org/10.1016/j.tws.2018.02.020.
[33] Samiee P, Niari SE, Ghandi E. Thermal and structural behavior of cold-formed steel frame wall under fire condition. Eng Struct 2022;252:113563. https://doi.org/10.1016/j.engstruct.2021.113563.
[34] Abeysiriwardena T, Mahendran M. Numerical modelling and fire testing of gypsum plasterboard sheathed cold-formed steel walls. Thin Walled Struct 2022;180:109792. https://doi.org/10.1016/j.tws.2022.109792.
[35] Ariyanayagam, A.D. and Mahendran, M., Behaviour of lsf walls exposed to fire on both sides. Proceedings of 3rd International Fire Safety Symposium, Ottawa, Ontario, Canada, 2019, pp. 137-145.
[36] Vy ST, Ariyanayagam A, Mahendran M. Behaviour and design of CFS stud walls under both sides fire exposure. Thin Walled Struct 2024;197:111619. https://doi.org/10.1016/j.tws.2024.111619.
[37] Inerhunwa, I., Hopkin, D., Kimbar, G., Spearpoint, M., Kanellopoulos, G., and Turkowski, P., Experimental study of the loadbearing performance of light gauge steel frame (lsf) walls exposed to fire on two sides. Proceedings of 13th International Conference on Structures in Fire SiF'24, University of Coimbra, Portugal, 2024, pp. 735-746.
[38] CROSS-UK, Fire protection to light gauge steel frame walls, CROSS-UK, UK, Report ID 1116, 2022. Available online: ⟨https://www.cross-safety.org/uk/safety-information/cross-safety-report/fire-protection-light-gauge-steel-frame-walls-1116⟩. (accessed on Aug. 08, 2024).
[39] Dodangoda MT, Mahendran M, Keerthan P, Frost RL. Developing a performance factor for fire rated boards used in LSF wall systems. Fire Saf J 2019;109:102872. https://doi.org/10.1016/j.firesaf.2019.102872.
[40] EN1993-1-3, Eurocode 3: Design of steel structures - Part 1-3: General rules - Supplementary rules for cold-formed members and sheeting [Authority: The European Union Per Regulation 305/2011, Directive 98/34/EC, Directive 2004/18/EC]. (2006), 130.
[41] Kankanamge ND, Mahendran M. Mechanical properties of cold-formed steels at elevated temperatures. Thin Walled Struct 2011;49:26–44. https://doi.org/10.1016/j.tws.2010.08.004.
[42] ANSYS®, Academic Research Mechanical, Release R2, 2023.
[43] Rokilan M, Mahendran M. Design of cold-formed steel wall studs subject to non-uniform elevated temperature distributions. Thin Walled Struct 2022;171:108625. https://doi.org/10.1016/j.tws.2021.108625.
[44] EN-1991-1-2, Eurocode 1: Actions on structures—Part 1-2: General actions—Actions on structures exposed to fire [Authority: The European Union Per Regulation 305/2011, Directive 98/34/EC, Directive 2004/18/EC]. British Standards, (2002), 58.
[45] Vieira Jr L, Schafer B. Behavior and design of sheathed cold-formed steel stud walls under compression. J Struct Eng 2013;139:772–86. https://doi.org/10.1061/(ASCE)ST.1943-541X.0000731.
[46] Schafer, B.W. and Ádány, S., Buckling analysis of cold-formed steel members using CUFSM: conventional and constrained finite strip methods. Proceedings of Eighteenth International Specialty Conference on Cold-Formed Steel Structures, Orlando, FL, 2006.
[47] Becque, J., The interaction of local and overall buckling of cold-formed stainless steel columns. (Ph.D. Thesis), The University of Sydney, Sydney, Australia, 2008.
[48] Schafer BW, Peköz T. Computational modeling of cold-formed steel: characterizing geometric imperfections and residual stresses. J Constr Steel Res 1998;47:193–210. https://doi.org/10.1016/S0143-974X(98)00007-8.
[49] AS/NZS4600, Cold-formed steel structures Australian/New Zealand Standard. Sydney, Australia, 1996.
[50] Ellobody E, Young B. Behavior of cold-formed steel plain angle columns. J Struct Eng 2005;131:457–66. https://doi.org/10.1061/(ASCE)0733-9445(2005)131:3(457).
[51] Gunalan, S., Structural behaviour and design of cold-formed steel wall systems under fire conditions. (PhD thesis), Faculty of built environment and engineering, Queensland University of Technology, 2011.
[52] EN1363-1. Fire resistance tests - Part 1: General requirements. Brussels, Belgium: CEN, European Committee for Standardization; 2020.
[53] Ariyanayagam AD, Mahendran M. Experimental study of load-bearing cold-formed steel walls exposed to realistic design fires. J Struct Fire Eng 2014;5:291–330. https://doi.org/10.1260/2040-2317.5.4.291.